



Equivalent in-plane dynamic elastic moduli of lattice structures with Plateau borders

X. Liu^{a,b,c,*}, L. Huang^{a,b,c}, S. Adhikari^d

^a Key Laboratory of Traffic Safety on Track, Ministry of Education, School of Traffic & Transportation Engineering, Central South University, Changsha, China

^b Joint International Research Laboratory of Key Technology for Rail Traffic Safety, Central South University, Changsha, China

^c National & Local Joint Engineering Research Center of Safety Technology for Rail Vehicle, Central South University, Changsha, China

^d James Watt School of Engineering, The University of Glasgow, Glasgow G12 8QQ, United Kingdom

ARTICLE INFO

Keywords:

Lattice with Plateau borders
Broadband dynamic homogenization
Equivalent dynamic elastic moduli
Dynamic stiffness method

ABSTRACT

Lattice structures with Plateau borders (LSPB) have attracted increasing interests recently due to the improved stiffness, strength, energy absorption properties. Undoubtedly, vertexes with Plateau borders (VPB) play a significant role on the dynamic elastic moduli. This paper proposes an analytical framework of the frequency-dependent equivalent in-plane dynamic elastic moduli (Young's moduli $E_1(\omega)$, $E_2(\omega)$, Poisson's ratio $\nu_{12}(\omega)$, $\nu_{21}(\omega)$ and shear modulus $G_{12}(\omega)$) of LSPB. First, dynamic stiffness (DS) matrix of a lattice cell edge (based on rod and Timoshenko theories) connected to VPBs (modelled as rigid bodies) at both ends is formulated. Then, based on the above DS matrix and the unit cell method, closed-form expressions of equivalent in-plane dynamic elastic moduli are proposed, which are sufficient general to be applied to four types of lattices. The effects of mass, inertia moment and size of VPB on the equivalent dynamic elastic moduli are studied, with both physical and mathematical interpretations. Furthermore, the proposed expressions are applied to honeycomb, rectangular, auxetic and rhombus LSPB and some interesting and important observations are made. This research provides analytical expressions for broadband dynamic elastic moduli of LSPB, which can be directly used in the design and optimization of composite structures with lattice cores.

1. Introduction

With excellent mechanical properties of light weight, high strength, high stiffness, high energy absorption rate and specific dynamic properties [1–9], lattice structures have been widely used in civil engineering, machinery, aerospace, transportation, and biomedicine applications as the cores of sandwich panels [10–16]. However, microstructural imperfections [17,18] are avoidable to be introduced in actual manufacturing process of lattice structures such as non-uniform cell-edge cross-section, non-straight cell edges, missing cells and non-periodic microstructures. It is clear that the mechanical properties (e.g., mass and stiffness distribution, geometry, etc.) of lattice structures are significantly affected by those preexisting microstructural imperfections and should therefore be considered in dynamic analysis. Vertexes with Plateau borders (VPB) in lattice structure are one of the most common imperfections as shown in Fig. 1. Essentially, the lattice structures can be treated as uniform cell edges (UCE) connected by VPB. The role-played by VPB on the dynamic elastic moduli is the main research target of this paper.

Since cell-edge bending is the primary deformation mechanism for lattice structures, it is expected that their mechanical properties are

affected by VPB. Some existing investigations have been conducted to study the effects of VPB on the stiffness [19], strength [19,20], compressive strength [21], elastic buckling strengths [22,23], failure surfaces [24–26], creep strain rate [27], plastic collapse strength [28] and wave propagation [29] of lattice structures. It is interesting to find that most of the above existing work [19–28,30] quantified the effect of VPB by an important parameter called the solid distribution [19,22], which is defined as the ratio of the volume of VPB over the total solid volume, i.e., $\phi_2 = \frac{A_p}{A_p + A_c}$ where A_p and A_c are defined in Fig. 1. Amongst these, Duan et al. [21] found that the square/hexagonal honeycombs with appropriate solid distribution can achieve more desirable compressive strength than the conventional square/hexagonal honeycombs through experimental analysis. Simone and Gibson [19] discussed the effects of solid distribution on the stiffness and strength of honeycomb lattice structures with Plateau borders using numerical method. Yang et al. [20] found that the discrepancies between the prediction and the FE predictions on the strength of regular hexagonal honeycombs became more significant

* Corresponding author at: Key Laboratory of Traffic Safety on Track, Ministry of Education, School of Traffic & Transportation Engineering, Central South University, Changsha, China.

E-mail addresses: xiangliu06@gmail.com (X. Liu), 1042642358@qq.com (L. Huang), Sondipon.Adhikari@glasgow.ac.uk (S. Adhikari).

<https://doi.org/10.1016/j.compstruct.2022.116056>

Received 6 December 2021; Received in revised form 21 June 2022; Accepted 4 August 2022

Available online 8 August 2022

0263-8223/© 2022 Elsevier Ltd. All rights reserved.

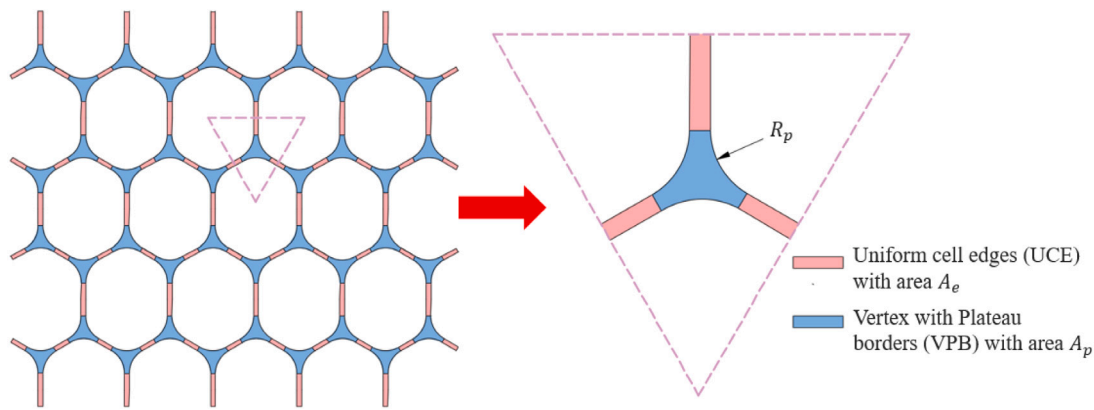


Fig. 1. Honeycomb lattice structures with Plateau borders and a repeating element composed of three uniform cell edges connected at a vertex with Plateau border. A_e is the area of the three uniform cell edges, and A_p is the area of the vertex with Plateau border.

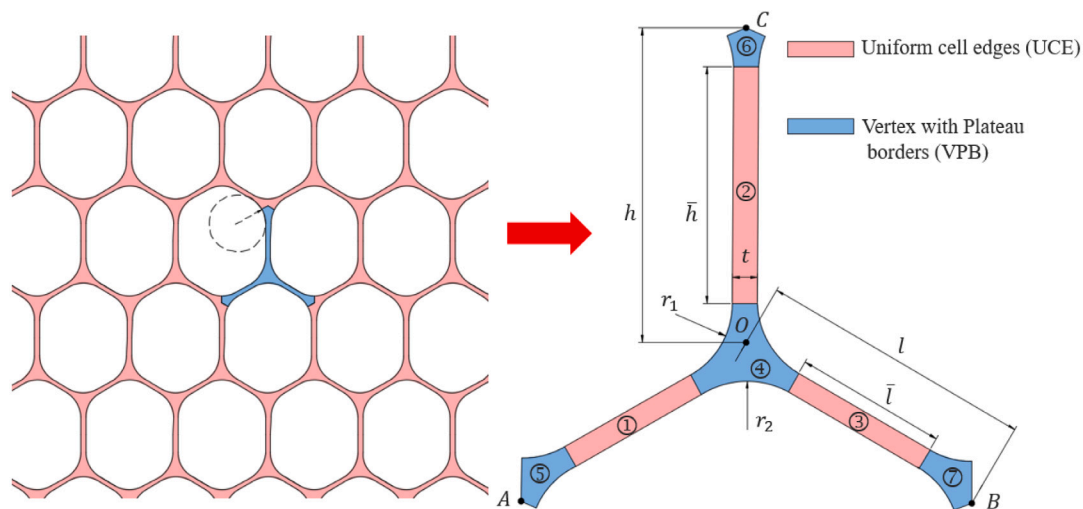


Fig. 2. A repeating unit cell of honeycomb lattice structures with Plateau borders.

for larger value of solid distribution. Chuang et al. [22,23] calculated the biaxial buckling strengths of regular hexagonal honeycombs with Plateau borders using finite element analysis. Yang et al. [24–26] evaluated the effects of the solid distribution on the failure surfaces, out-of-plane elastic properties of honeycombs with Plateau borders. Lin et al. [27] studied the effects of the solid distribution on the creep strain rate of hexagonal honeycombs. Chuang et al. [28] focused on the effects of solid distribution on the elastic moduli and plastic collapse strength of hexagonal honeycombs. Zhang et al. [29] investigate the plane wave propagation in hexagonal lattices with plateau borders and analyse the effects of the dimensional parameters on the dynamic properties of hexagonal lattices. However, the lattice structures often work in vibrating system such as aerospace, high-speed trains, wind turbines, electro-mechanical devices, base-isolation devices [31,32] and so on, and sporadic research have been reported the dynamic mechanical properties of the lattice structures with Plateau borders in a vibrating environment. In a vibrating condition, deformation behaviour of lattice structures becomes significantly different from the behaviour under a static condition. Undoubtedly, the VPBs have significant mass, inertia moment and stiffness which will play an important role on the dynamic elastic moduli of the lattice structures. Similar with the above research [19–29], the effect of solid distribution on the dynamic elastic moduli is an important and interesting topic. To the best knowledge of authors, the effect of the mass, inertia moment and stiffness of VPB on the dynamic elastic moduli has not been studied.

Although it is possible to build a detailed finite element (FE) model for the lattice structures with Plateau borders, the FE model will contain

a large number of repeating elements leading to high computing costs. This will become very inefficient and less feasible for the dynamic analysis of complex built-up structures. Alternatively, the macro-mechanics parameters of lattice structures can be represented by equivalent mechanical and density properties based on either experiments [33,34] or simulations [17,35,36]. Recently, a data-driven multilevel computational homogenization (FE²) [37–39] opens up the fusion channel between simulations and experiments, which provides a uniform and powerful framework with strong engineering versatility for the structural analysis of composite materials. It is well-known that equivalent dynamic parameters of lattice structures (such as stiffness, Poisson's ratios) are always frequency-dependent in nature. Of course, the equivalent properties obtained from experiments are very convincing, but the results are very sensitive to experiment settings [40] and it is inconvenient to manufacture a large number of samples for the parametrical studies and optimization design. Therefore, many other researchers proposed equivalent static elastic moduli and equivalent density parameters of lattice structures based on homogenization methods by using analytical methods [41–43]. Then, dynamic analysis on lattice structures could be performed [44,45]. However, these predictions based on equivalent static elastic moduli and equivalent density parameters are accurate only at low frequency due to the difficulty in capturing the medium to high frequency dynamic behaviour [46]; Moreover, it cannot give specific expressions and necessary physical insights. The above shortcoming of static homogenization can be overcome by a dynamic homogenization method [47] for the purpose of broadband

dynamic predictions of lattice structures. In more specific, the dynamic homogenization is performed by combing the unit cell method (or representative volume element) [41,48–50] and the analytical dynamic stiffness (DS) method [51–60]. The unit cell method helps to describe the equivalent macro-mechanical properties by using micro-mechanical properties based on a unit cell, whereas the DS method describes the broadband dynamic deformation of lattice edges by using very few degrees of freedom without resorting to discretization. Generally speaking, there are two ways to develop the homogenization model for lattice structures based on unit cell method, namely, (1) application of boundary displacements leading to forces [49,61,62]; and (2) application of boundary stress excitations leading to displacement [41,46,47]. Following either of those two methods, the constitutive relationships of stress and strain could be obtained. By using the latter method, Adhikari and his co-authors [46,47,63] have proposed an analytical framework of the equivalent frequency-dependent elastic moduli of lattice structures based on the unit cell method and DS formulations. The analytical expressions of the equivalent dynamic elastic moduli are (1) suitable for both statics and dynamics analysis within a broadband frequency range; (2) quite general to be applied to a wide range of different types of lattices; (3) in analytical sense which are easy to be understood from both physical and mathematical aspects. However, it is obvious a challenging task to develop the equivalent frequency-dependent elastic moduli of lattice structures with VPB, due to the non-uniform cell edges as well as the significant effects of VPB for the dynamic behaviours. Existing research for modelling lattice structures with VPB are generally either based on very fine mesh with large number of Dofs [20,26], or rigid equilateral triangular joint in static analysis [23,25,27]. Nevertheless, the dynamic homogenization of lattice structures with Plateau borders has not been carried out in spite of its great importance in engineering application as mentioned earlier.

In the present work, based on the unit cell method combined with dynamic stiffness (DS) method, this paper develops an analytical framework for the equivalent dynamic elastic moduli of lattice structures with Plateau borders. First, the vertex with Plateau border (VPB) is modelled by rigid bodies with mass, inertia moment and size properties, whereas the uniform cell edges (UCE) are described by the exact dynamic stiffness matrices based on rod and Timoshenko theories (see Section 2). The close-form DS matrix of UCE connected to VPBs at both ends is formulated based on a formulation procedure of multi-body dynamic systems (see Section 2). Then the analytical expressions of equivalent dynamic elastic moduli of lattice structures with Plateau border is derived by based on the unit cell approach and the above developed DS matrix (see Section 3). In particular, the derivation of equivalent dynamic shear modulus is based on a unique but more reasonable unit cell compared to existing research [47], where the equilibrium of both joints and unit cells is satisfied (see Section 3.1.2). Then the effect of mass, inertia moment and size (stiffness) of VPB on equivalent dynamic elastic moduli of lattice structures are systematically investigated and explained with mathematical and physical interpretations in Section 4. Next the effect of VPB on the equivalent dynamic elastic moduli of four types of lattice structures including honeycomb, rectangular, auxetic and rhombus lattice structures are studied in Section 5. Section 6 provides the concluding remarks.

2. Dynamic stiffness matrix of a unit cell with Plateau borders

This paper focuses on developing the frequency-dependent equivalent dynamic elastic moduli which are analytically expressed based on the dynamic stiffness method following the concept proposed in [47]. The equivalent properties of lattice structures can be determined based on a repeating unit cell [41,64–66]. This is acceptable within the scope of asymptotic homogenization theory as long as other unit cells behave in the same way under the same loading condition. Since the unit cells are identical in nature, this is the case. It is, however, a requirement that the dynamics of the system must be in a steady state (that is, no

transients are allowed). The choice of the unit cell is not unique, as long as it physically represents the entire lattice structure [47,49,67,68].

As shown in Fig. 2, a unit cell is selected from the entire lattices with Plateau borders. The unit cell consists of vertex with Plateau borders (VPB) ④, the divided VPBs ⑤, ⑥, ⑦, vertical uniform cell edges (UCE) ② and inclined UCes ①, ③. Nodes *A, B, C, D* are mass centres of those VPBs. The connections between UCes and VPBs are essentially rigid connections. For such a model, some reasonable assumptions can be made: (1) The stiffness of VPBs is much larger than the stiffness of inclined or vertical UCes and therefore can be treated as rigid bodies. (2) The mass *m* and inertia moment *I* of VPBs play important role in the dynamic behaviours of the lattice structures and cannot be ignored. (3) The distance between the mass centre of VPB to the centre of the rigid connection should be taken into account.

Next we will derive the dynamic stiffness matrix for a typical VPB ⑤-UCE ①-VPB ④ in Fig. 3 as an illustrative example. The derivation follows a similar procedure proposed by the first author recently [69]. In Fig. 3, the nodes of the divided VPB ⑤ are *A* and *D*. Through balance and geometric relationship, the force and displacement relationship between nodes *A* and *D* can be obtained as

$$\begin{aligned} N_A &= N_D \\ V_A &= V_D \\ M_A &= M_D + V_D \Delta x - N_D \Delta y \\ U_D &= U_A - \theta_A \Delta y \\ W_D &= W_D + \theta_A \Delta x \\ \theta_D &= \theta_A \end{aligned} \quad (1)$$

Similarly, for VPB ④, the force and displacement relationship between nodes *O* and *E* can also be given as

$$\begin{aligned} N_O &= N_E \\ V_O &= V_E \\ M_O &= M_E - V_E \Delta x + N_E \Delta y \\ U_E &= U_O + \theta_E \Delta y \\ W_E &= W_O - \theta_E \Delta x \\ \theta_E &= \theta_O \end{aligned} \quad (2)$$

UCes are of high aspect ratio which are modelled as flexible beam elements. Thus, the force and displacement relationship in the frequency domain between nodes *D* and *E* of the inclined UCE ① can be formulated in the dynamic stiffness matrix in the form

$$\begin{bmatrix} N_D \\ V_D \\ M_D \\ N_E \\ V_E \\ M_E \end{bmatrix} = \begin{bmatrix} a_1 & 0 & 0 & a_2 & 0 & 0 \\ 0 & d_1 & d_2 & 0 & d_4 & d_5 \\ 0 & d_2 & d_3 & 0 & -d_5 & d_6 \\ a_2 & 0 & 0 & a_1 & 0 & 0 \\ 0 & d_4 & -d_5 & 0 & d_1 & -d_2 \\ 0 & d_5 & d_6 & 0 & -d_2 & d_3 \end{bmatrix} \begin{bmatrix} U_D \\ W_D \\ \theta_D \\ U_E \\ W_E \\ \theta_E \end{bmatrix} \quad (3)$$

where a_1 and a_2 are dynamic stiffness coefficients for axial deformation of beam elements of the inclined member *DE* of length \bar{l} . $d_1 - d_6$ are stiffness coefficients for bending deformation of the beam element *DE*. Their derivations based on both classical rod and Timoshenko beam theories are given in Appendices A and B for the sake of self-containedness.

Finally, eliminating the force and displacement relationship between nodes *D* and *E* based on Eqs. (1)–(3), the relationship between nodes *A* and *O* can be expressed in the form of dynamic stiffness matrix following the formulation procedure in [69]

$$\begin{bmatrix} N_O \\ V_O \\ M_O \\ N_A \\ V_A \\ M_A \end{bmatrix} = \begin{bmatrix} K_{11}^{OA}(\omega) & 0 & 0 & K_{14}^{OA}(\omega) & 0 & K_{16}^{OA}(\omega) \\ & K_{22}^{OA}(\omega) & K_{23}^{OA}(\omega) & 0 & K_{25}^{OA}(\omega) & K_{26}^{OA}(\omega) \\ & & K_{33}^{OA}(\omega) & 0 & K_{35}^{OA}(\omega) & K_{36}^{OA}(\omega) \\ & & & K_{44}^{OA}(\omega) & 0 & K_{46}^{OA}(\omega) \\ & & & & K_{55}^{OA}(\omega) & K_{56}^{OA}(\omega) \\ & & & & & K_{66}^{OA}(\omega) \end{bmatrix} \begin{bmatrix} U_O \\ W_O \\ \theta_O \\ U_A \\ W_A \\ \theta_A \end{bmatrix} \quad (4)$$

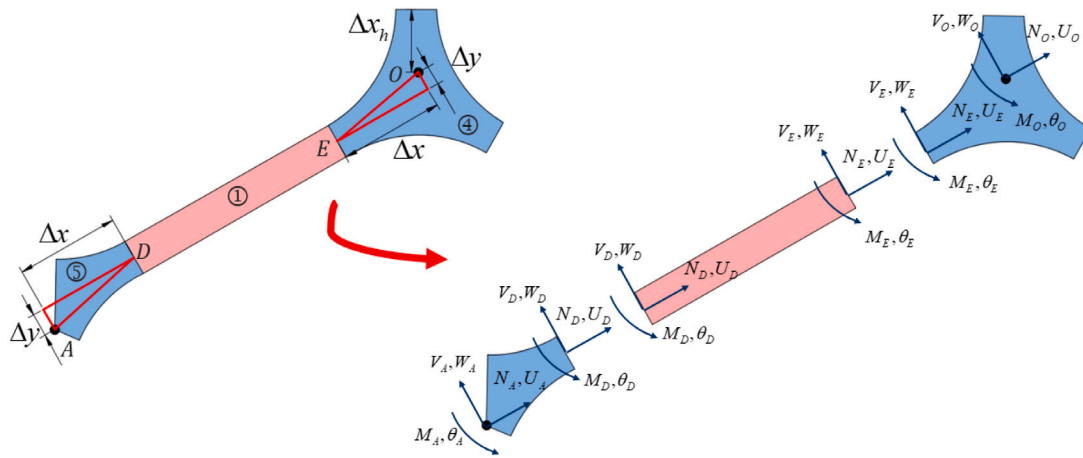


Fig. 3. Inclined component consisting of the divided VPB ⑤ -UCE ① -VPB ③. N_i, V_i and M_i represent the axial force, shear force and bending moment at node i ($i = A, D, E, O$), respectively; U_i, W_i and θ_i represent amplitudes of the axial displacement, the vertical or bending displacement, and the angular or bending rotation at node i ($i = A, D, E, O$), respectively. Δx is the distance between the mass centre of VPB and the geometric centre of the rigid connection in the direction of inclined member. Δy is the distance between the mass centre of VPB and the geometric centre of the rigid connection in the direction perpendicular to the inclined member.

where

$$\begin{aligned} K_{11}^{OA}(\omega) &= a_1 - m\omega^2, K_{22}^{OA}(\omega) = d_1 - m\omega^2, K_{33}^{OA}(\omega) = d_3 - I\omega^2 \\ K_{44}^{OA}(\omega) &= a_1 - \varphi m\omega^2, K_{55}^{OA}(\omega) = d_1 - \varphi m\omega^2, K_{66}^{OA}(\omega) = \bar{d}_3 - \varphi I\omega^2 \\ K_{14}^{OA}(\omega) &= a_2, K_{16}^{OA}(\omega) = a_2\Delta y, K_{23}^{OA}(\omega) = -\bar{d}_2 \\ K_{25}^{OA}(\omega) &= \bar{d}_4, K_{26}^{OA}(\omega) = -\bar{d}_5, K_{35}^{OA}(\omega) = -\bar{d}_5 \\ K_{36}^{OA}(\omega) &= \bar{d}_6 + \bar{d}_5\Delta x, K_{46}^{OA}(\omega) = a_1\Delta y, K_{56}^{OA}(\omega) = -\bar{d}_2 \end{aligned} \quad (5)$$

and

$$\begin{aligned} \bar{d}_2 &= d_1\Delta x + d_2 \\ \bar{d}_3 &= d_1\Delta x^2 + 2d_2\Delta x + d_3 + a_1\Delta y^2 \\ \bar{d}_5 &= -d_4\Delta x + d_5; \bar{d}_6 = d_5\Delta x + d_6 \end{aligned} \quad (6)$$

In this matrix, φ is the ratio between the area of the divided VPB ⑤ to that of VPB ④. We also define φ_h is the ratio between the area of the divided VPB ⑥ to that of VPB ④. m and I are the mass and inertia moment of VPB ④. Using the same method, the force and displacement relationship between nodes O and C can also be obtained. It should be noted that the shape of the VPBs can be arbitrarily defined in a sufficiently general manner, which provides the possibility to study the equivalent dynamic elastic moduli of different types of lattices.

3. Equivalent dynamic elastic moduli of lattice structures with Plateau borders

Section 2 has proposed the dynamic stiffness matrix of a unit cell with Plateau borders. In order to derive the equivalent dynamic elastic moduli of lattice structures with Plateau borders, the derivation of equivalent dynamic elastic moduli based on unit cell equilibrium is given in Section 3.1. Based on the work of Sections 2 and 3.1, the analytical expressions of equivalent dynamic elastic moduli are given in Section 3.2.

3.1. Equivalent elastic moduli based on a unit cell

The objective of this section is to express equivalent in-plane elastic moduli of the lattice structures in terms of the dynamic stiffness matrix coefficients using the unit cell approach. It should be noted that the expressions of Young's moduli $E_1(\omega), E_2(\omega)$ and Poisson's ratio $\nu_{12}(\omega)$ and $\nu_{21}(\omega)$ are in the same form as [47], whereas that of the shear modulus $G_{12}(\omega)$ is different. The derivation of $G_{12}(\omega)$ is based on different but more physically reasonable unit cell compared to [47].

3.1.1. Review of Young's moduli and Poisson's ratios

For the sake of self-containedness, the derivations of the analytical expressions for in-plane dynamic elastic moduli $E_1(\omega), E_2(\omega), \nu_{12}(\omega)$ and $\nu_{21}(\omega)$ [47] are reviewed briefly as follows.

As shown in Fig. 4(a), the model is used to derive the Young's moduli $E_1(\omega)$ and Poisson's ratio $\nu_{12}(\omega)$ in direction-1. Uniform harmonic stress $\sigma_1(\omega)e^{i\omega t}$ is applied in direction-1, resulting in nodes A and B to be applied at harmonic force $F_1 = F_1(\omega)e^{i\omega t}$, here

$$F_1(\omega) = \sigma_1(\omega)b(h + l \sin \theta) \quad (7)$$

where b is the height of lattice structure, θ is the cell angle. Since the deformations of inclined members OA and OB are symmetric about OC , only OA is needed for analysis. At node A , $F_1(\omega)$ can be decomposed into $F_1(\omega) \cos \theta$ and $F_1(\omega) \sin \theta$ along the axial and transverse directions of OA . γ and η are the deformations transverse and along the inclined member AO . According to [47], the strain in direction-1 can be given as

$$\varepsilon_1(\omega) = \frac{\delta_1(\omega)}{l \cos \theta} = \frac{\sigma_1(\omega) b (h/l + \sin \theta) \sin^2 \theta}{K_{55}^{OA}(\omega) \cos \theta} \left(1 + \cot^2 \theta \frac{K_{55}^{OA}(\omega)}{K_{44}^{OA}(\omega)} \right) \quad (8)$$

Therefore, the Young's moduli $E_1(\omega)$ is obtained as

$$E_1(\omega) = \frac{\sigma_1(\omega)}{\varepsilon_1(\omega)} = \frac{K_{55}^{OA}(\omega) \cos \theta}{b (h/l + \sin \theta) \sin^2 \theta \left(1 + \cot^2 \theta \frac{K_{55}^{OA}(\omega)}{K_{44}^{OA}(\omega)} \right)} \quad (9)$$

The strain in direction-2 is

$$-\varepsilon_2(\omega) = \frac{-\delta_2(\omega)}{h + l \sin \theta} = \frac{\sigma_1 b \sin \theta \cos \theta}{K_{55}^{OA}(\omega)} \left(1 - \frac{K_{55}^{OA}(\omega)}{K_{44}^{OA}(\omega)} \right) \quad (10)$$

After calculating the strains $\varepsilon_1(\omega)$ and $\varepsilon_2(\omega)$ in direction-1 and direction-2, the Poisson's ratio can be obtained as

$$\nu_{12}(\omega) = -\frac{\varepsilon_2(\omega)}{\varepsilon_1(\omega)} = \frac{\cos^2 \theta \left(1 - \frac{K_{55}^{OA}(\omega)}{K_{44}^{OA}(\omega)} \right)}{(h/l + \sin \theta) \sin \theta \left(1 + \cot^2 \theta \frac{K_{55}^{OA}(\omega)}{K_{44}^{OA}(\omega)} \right)} \quad (11)$$

Similarly, the model shown in Fig. 4(b) is used to derive Young's moduli $E_2(\omega)$ and Poisson's ratio $\nu_{21}(\omega)$ in direction-2. γ and η are the deformations transverse and along the inclined member AO . δ_0 is the displacement of point O in the 2-direction arising from the axial deformation of the vertical member OC . We can arrive at

$$E_2(\omega) = \frac{\sigma_2(\omega)}{\varepsilon_2(\omega)} = \frac{K_{55}^{OA}(\omega) (h/l + \sin \theta)}{b \cos^3 \theta \left(1 + \tan^2 \theta \frac{K_{55}^{OA}(\omega)}{K_{44}^{OA}(\omega)} + \frac{2K_{55}^{OA}(\omega)}{\cos^2 \theta K_{44}^{OA}(\omega)} \right)} \quad (12)$$

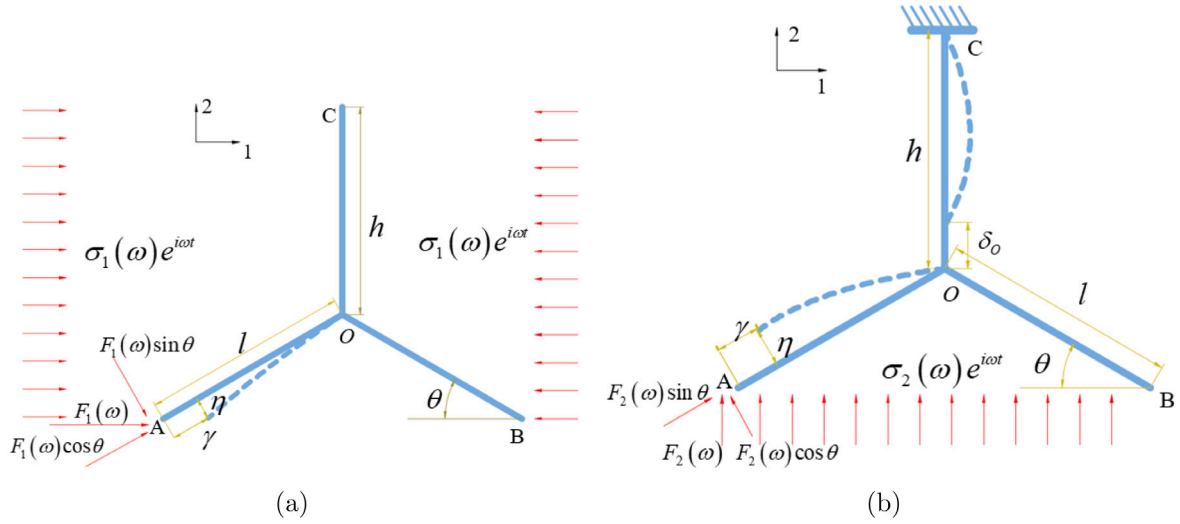


Fig. 4. (a) In order to derive $E_1(\omega)$ and $\nu_{12}(\omega)$, uniform harmonic stress $\sigma_1(\omega)e^{i\omega t}$ is applied in direction-1. (b) In order to derive $E_2(\omega)$ and $\nu_{21}(\omega)$, uniform harmonic stress $\sigma_2(\omega)e^{i\omega t}$ is applied in direction-2.

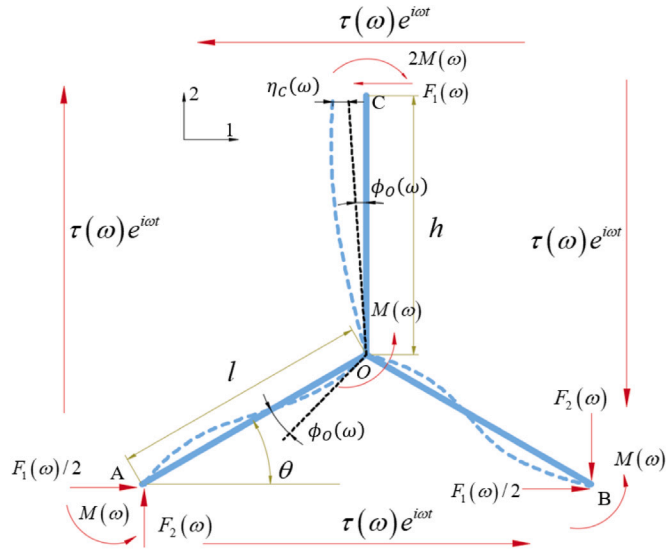


Fig. 5. Improved dynamic equilibrium and deformation patterns of the unit cell under the application of the harmonic shear stress field $\tau(\omega)e^{i\omega t}$, which is used for deriving the in-plane shear modulus $G_{12}(\omega)$.

$$\nu_{21}(\omega) = \frac{-\varepsilon_1(\omega)}{\varepsilon_2(\omega)} = \frac{(h/l + \sin \theta) \sin \theta \left(1 - \frac{K_{55}^{OA}(\omega)}{K_{44}^{OA}(\omega)}\right)}{\cos^2 \theta \left(1 + \tan^2 \theta \frac{K_{55}^{OA}(\omega)}{K_{44}^{OA}(\omega)} + \frac{2K_{55}^{OA}(\omega)}{\cos^2 \theta K_{44}^{OC}(\omega)}\right)} \quad (13)$$

3.1.2. Shear modulus $G_{12}(\omega)$ based on a novel unit cell

In the derivation of the in-plane equivalent shear modulus $G_{12}(\omega)$, the novel model used in this work has the following differences compared with [47]: (1) [47] requires two unit cells as shown in Appendix C, while this paper requires only one unit cell as shown in Fig. 5. (2) The equilibrium of both joints and unit cells is satisfied in the present analysis model while the analysis model of [47] cannot satisfy equilibrium strictly. Therefore, the cell model used in this paper is simpler and more physically reasonable.

In order to derive the shear modulus $G_{12}(\omega)$, we put forward three assumptions: (1) Nodes A, O and B have no relative displacements [41,

46]. (2) Each node rotates at the same angle. (3) The shear deformation is caused by the bending deformation of OC and its deflection due to rotation of node O arising from the bending of OA.

First, the bending deformation of OC can be obtained as

$$\eta_C(\omega) = \frac{K_{66}^{OC}(\omega) F_1(\omega) + 2K_{56}^{OC}(\omega) M(\omega)}{K_{55}^{OC}(\omega) K_{66}^{OC}(\omega) - K_{56}^{OC}(\omega) K_{65}^{OC}(\omega)} \quad (14)$$

Then according to the equilibrium of OA, the rotation angle of node O arising from the bending of OA is

$$\phi_O(\omega) = \frac{M(\omega) (K_{66}^{OA}(\omega) - K_{36}^{OA}(\omega))}{K_{33}^{OA}(\omega) K_{66}^{OA}(\omega) - K_{36}^{OA}(\omega) K_{63}^{OA}(\omega)} \quad (15)$$

According to the equilibrium, we can obtain

$$M(\omega) = \frac{F_1(\omega)h}{4} \quad (16)$$

Therefore the total shear deformation is given as

$$\begin{aligned} \gamma_1 &= (\phi_O(\omega) h + \eta_C(\omega)) \\ &= F_1(\omega) \left(\frac{2K_{66}^{OC}(\omega) + hK_{56}^{OC}(\omega)}{2(K_{55}^{OC}(\omega)K_{66}^{OC}(\omega) - (K_{56}^{OC}(\omega))^2)} + \frac{(K_{66}^{OA}(\omega) - K_{36}^{OA}(\omega))h^2}{4[K_{33}^{OA}(\omega)K_{66}^{OA}(\omega) - K_{36}^{OA}(\omega)K_{63}^{OA}(\omega)]} \right) \end{aligned} \quad (17)$$

The total shear strain is

$$\gamma(\omega) = \frac{\gamma_1}{h + l \sin \theta} \quad (18)$$

Then the shear modulus $G_{12}(\omega)$ is expressed as

$$\begin{aligned} G_{12} &= \frac{\tau(\omega)}{\gamma(\omega)} \\ &= \frac{(h + l \sin \theta)}{bl \cos \theta \left(\frac{2K_{66}^{OC}(\omega) + hK_{56}^{OC}(\omega)}{K_{55}^{OC}(\omega)K_{66}^{OC}(\omega) - (K_{56}^{OC}(\omega))^2} + \frac{(K_{66}^{OA}(\omega) - K_{36}^{OA}(\omega))h^2}{2[K_{33}^{OA}(\omega)K_{66}^{OA}(\omega) - K_{36}^{OA}(\omega)K_{63}^{OA}(\omega)]} \right)} \end{aligned} \quad (19)$$

In particular, for the unit cell of lattice structures without Plateau borders

$$K_{36}^{OA}(\omega) = K_{63}^{OA}(\omega), K_{33}^{OA}(\omega) = K_{66}^{OA}(\omega) \quad (20)$$

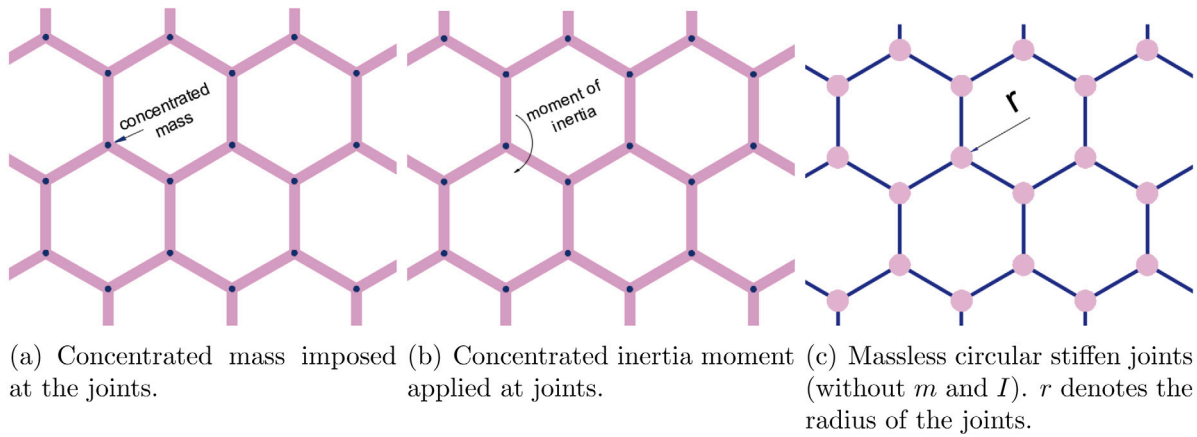


Fig. 6. Unit cells used for studying the effect of VPB.

The above equation can be simplified as

$$G_{12} = \frac{\tau(\omega)}{\gamma(\omega)} = \frac{(h/l + \sin \theta)}{bl \cos \theta \left(\frac{2K_{66}^{OC}(\omega) + hK_{56}^{OC}(\omega)}{K_{55}^{OC}(\omega)K_{66}^{OC}(\omega) - (K_{56}^{OC}(\omega))^2} + \frac{h^2}{2(K_{66}^{OA}(\omega) + K_{63}^{OA}(\omega))} \right)} \quad (21)$$

3.2. Analytical expressions of equivalent dynamic elastic moduli

In Section 2, Eq. (5) provides the dynamic stiffness coefficients of OA (K_{ij}^{OA}). K_{ij}^{OC} can be also obtained using the same method. By substituting these dynamic stiffness coefficients into Eqs. (9), (11), (12), (13), (19), the analytical expressions of equivalent in-plane dynamic elastic moduli can be summarized as

$$E_1(\omega) = \frac{\cos \theta}{b(h/l + \sin \theta) \sin^2 \theta} \frac{d_1 - \varphi m \omega^2}{\left(1 + \cot^2 \theta \frac{d_1 - \varphi m \omega^2}{a_1 - \varphi m \omega^2}\right)} \quad (22)$$

$$v_{12}(\omega) = \frac{\cos^2 \theta}{(h/l + \sin \theta) \sin \theta} \frac{1 - \frac{d_1}{a_1}}{\left(1 + \frac{d_1}{a_1} \cot^2 \theta - \frac{\varphi m \omega^2 \csc^2 \theta}{a_1}\right)} \quad (23)$$

$$E_2(\omega) = \frac{h/l + \sin \theta}{b \cos^3 \theta} \frac{d_1 - \varphi m \omega^2}{\left(1 + \tan^2 \theta \frac{d_1 - \varphi m \omega^2}{a_1 - \varphi m \omega^2} + \frac{2(d_1 - \varphi m \omega^2)}{\cos^2 \theta (a_1^h - \varphi m \omega^2)}\right)} \quad (24)$$

$$v_{21}(\omega) = \frac{(h/l + \sin \theta) \sin \theta}{\cos^2 \theta} \times \frac{1 - \frac{d_1}{a_1}}{\left(1 + \frac{d_1}{a_1} \tan^2 \theta - \frac{\varphi m \omega^2 \sec^2 \theta}{a_1} + \frac{2(a_1 - \varphi m \omega^2)(d_1 - \varphi m \omega^2)}{a_1 (a_1^h - \varphi m \omega^2) \cos^2 \theta}\right)} \quad (25)$$

$$G_{12}(\omega) = \frac{(h/l + \sin \theta)}{b \cos \theta \left(\frac{h \bar{d}_3 + 2 \bar{d}_1 - 2 \varphi_n l \omega^2}{(\bar{d}_1^h - \varphi_n m \omega^2)(\bar{d}_3^h - \varphi_n l \omega^2) - (\bar{d}_2^h)^2} + \frac{h^2 (\bar{d}_3 - \bar{d}_6 - \bar{d}_5 \Delta x - \varphi l \omega^2)}{2((\bar{d}_3 - \varphi l \omega^2)(\bar{d}_3 - l \omega^2) - (\bar{d}_6 + \bar{d}_5 \Delta x)^2)} \right)} \quad (26)$$

When $m = 0$, $I = 0$, $\Delta x = 0$, $\Delta y = 0$, $\Delta x_h = 0$, $\Delta y_h = 0$ in Eqs. (22)–(26), the equivalent dynamic elastic moduli of lattice structures without Plateau borders are obtained, which are the same as [47] except for the shear modulus based on a different unit cell, namely

$$E_{1ns}(\omega) = \frac{\cos \theta}{b(h/l + \sin \theta) \sin^2 \theta} \frac{d_1}{\left(1 + \cot^2 \theta \frac{d_1}{a_1}\right)} \quad (27)$$

$$v_{12ns}(\omega) = \frac{\cos^2 \theta}{(h/l + \sin \theta) \sin \theta} \frac{1 - \frac{d_1}{a_1}}{\left(1 + \frac{d_1}{a_1} \cot^2 \theta\right)} \quad (28)$$

$$\bar{E}_{2ns}(\omega) = \frac{h/l + \sin \theta}{b \cos^3 \theta} \frac{d_1}{\left(1 + \tan^2 \theta \frac{d_1}{a_1} + \frac{2d_1}{\cos^2 \theta a_1^h}\right)} \quad (29)$$

$$v_{21ns}(\omega) = \frac{(h/l + \sin \theta) \sin \theta}{\cos^2 \theta} \frac{1 - \frac{d_1}{a_1}}{\left(1 + \frac{d_1}{a_1} \tan^2 \theta + \frac{2d_1}{a_1^h \cos^2 \theta}\right)} \quad (30)$$

$$G_{12ns}(\omega) = \frac{(h/l + \sin \theta)}{b \cos \theta \left(\frac{-\bar{r}_h}{d_1^h a_3^h - (d_2^h)^2} + \frac{h^2}{2(\bar{d}_3 + \bar{d}_6)} \right)} \quad (31)$$

It should be noted that the above formulations are applicable in the relatively low frequency region so that the global wavelength is much larger than the size of a unit cell (since in engineering practice, the size of the unit cell is normally much smaller than the overall geometry of the lattice core, this is a reasonable assumption). In such a case, the periodic nature of the stress/displacement is valid as the global waveform is smooth and effectively uniform within a unit cell.

4. The effect of Plateau borders on the equivalent dynamic elastic moduli

In Section 3, we have obtained the analytical expressions of equivalent in-plane dynamic elastic moduli of lattice structures with Plateau borders. The objective of this section is to investigate the role-played by the vertex with Plateau borders (VPB), which are quantified by the mass m , inertia moment I and size (stiffness) of VPB. Then the dependence of these factors on the dynamic elastic moduli of different types of lattice structures is discussed in Section 5.

The geometric parameters of lattice structures and intrinsic material properties are taken as: $t/l = 0.1$, $b = 0.05$ mm, $E = 2 \times 10^3$ N/mm², $\rho = 7800$ kg/m³, the Poisson's ratio of the underlying material $\nu = 0.3$. For uniform cell edges (UCE) based on classical rod and Timoshenko beam theories in Appendices A and B, shear factor $k = 5/6$, damping value $c_m = 10^{-2}$ and $c_k = 10^{-5}$.

To interpret the results more clearly, this paper put forward the following instructions: (1) The equivalent dynamic elastic moduli are plotted in the form of a three-dimensional graph. (i.e. The z -coordinate corresponds to the equivalent elastic moduli, and the x/y -coordinate for normalized frequency/other parameters). (2) The local maximum/minimum of elastic moduli corresponds to the anti-resonance/resonance point. (3) For comparative purposes, the equivalent dynamic elastic moduli of lattice structures without Plateau borders are denoted by $E_{1ns}(\omega)$, $E_{2ns}(\omega)$, $v_{12ns}(\omega)$, $v_{21ns}(\omega)$ and $G_{12ns}(\omega)$. (4) In Sections 4 and 5, the results of this paper are sometimes compared with the following

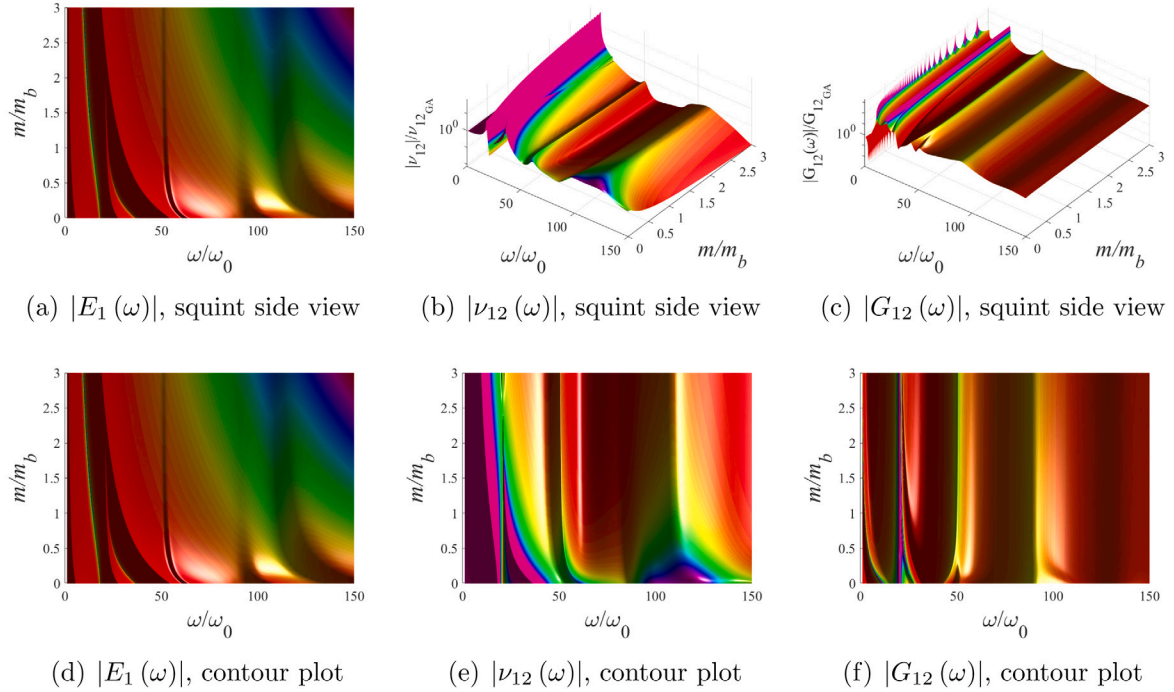


Fig. 7. The equivalent dynamic elastic moduli are normalized with respect to their corresponding static elastic moduli in Eqs. (32), (34) and (36). Absolute value of the results are plotted as functions of the normalized frequency ω/ω_0 for different m/m_b . Here $t/l = 0.1$, $h/l = 1$ and $\theta = \pi/6$.

static elastic moduli [41]

$$E_{1GA} = E\alpha^3 \frac{\cos \theta}{(\beta + \sin \theta) \sin^2 \theta} \quad (32)$$

$$E_{2GA} = E\alpha^3 \frac{(\beta + \sin \theta)}{\cos^3 \theta} \quad (33)$$

$$\nu_{12GA} = \frac{\cos^2 \theta}{(\beta + \sin \theta) \sin \theta} \quad (34)$$

$$\nu_{21GA} = \frac{(\beta + \sin \theta) \sin \theta}{\cos^2 \theta} \quad (35)$$

$$G_{12GA} = E\alpha^3 \frac{(\beta + \sin \theta)}{\beta^2(1 + 2\beta) \cos \theta} \quad (36)$$

where

$$\alpha = \frac{t}{l}, \beta = \frac{h}{l} \quad (37)$$

In order to investigate the roles played by the VPB on the equivalent dynamic elastic moduli, we propose three representative cases as shown in Fig. 6. In Fig. 6(a), m is imposed at the joints, whereas in Fig. 6(b) I is applied at the joints. In order to study the effect of the size of VPB, the massless stiffened circular joints (without m and I) is used for analysis in Fig. 6(c), where the radius of stiffened circular joints is r . Then we discuss the roles played by the three parameters, respectively. Here, we consider the special case of lattice structures with $h/l = 1$, $\bar{h}/\bar{l} = 1$ and $\theta = \pi/6$, it is therefore expected that $E_1(\omega) = E_2(\omega)$ and $\nu_{12}(\omega) = \nu_{21}(\omega)$ as shown in Eqs. (38) and (39).

$$E_1(\omega) = E_2(\omega) = \frac{4\sqrt{3}}{3} \frac{d_1 - \varphi m \omega^2}{\left(1 + 3 \frac{d_1 - \varphi m \omega^2}{a_1 - \varphi m \omega^2}\right)} \quad (38)$$

$$\nu_{12}(\omega) = \nu_{21}(\omega) = \frac{1 - \frac{d_1}{a_1}}{1 + 3 \frac{d_1}{a_1} - 4 \frac{\varphi m \omega^2}{a_1}} \quad (39)$$

Thus, there is no need to give all 5 equivalent in-plane dynamic elastic moduli, we only look at $E_1(\omega)$, $\nu_{12}(\omega)$ and $G_{12}(\omega)$.

4.1. Effect of mass of VPB on equivalent dynamic elastic moduli

In Fig. 6(a), concentrated mass m is imposed at the joints. The absolute value of equivalent dynamic elastic moduli is plotted in Fig. 7. m_b is the mass of UCE with length l . ω_0 is the first-order natural frequency of transverse vibration of simply supported UCE with length l (i.e. $\omega_o = \sqrt{\frac{EI}{\rho A l^4}}$). We also made comparisons to demonstrate the differences with static equivalent elastic moduli of Eqs. (32), (35) and (36). A three-dimensional surface diagrams from two different perspectives are given in Fig. 7.

A closer look at Fig. 7 reveals that: (1) The effect of m on Young's moduli and Poisson's ratio is relatively significant, while that on the shear modulus is not so obvious. This is expected since the mass of VPB only affects the stiffness coefficients $K_{44}^{OA}(\omega)$ and $K_{55}^{OA}(\omega)$ in Eq. (5) and subsequently $E_1(\omega)$ and $\nu_{12}(\omega)$. In comparison, $G_{12}(\omega)$ is only affected by $K_{55}^{OA}(\omega)$ and other stiffness coefficients which are not affected by m . (2) The effect of m on the equivalent dynamic elastic moduli is relatively large 0–0.5 m/m_b , while the trend is stable for 0.5 m/m_b and higher. (3) When ω/ω_0 is greater than 50, the equivalent dynamic elastic moduli changes monotonically with the increase of m . It is completely expected due to the inertia effect.

4.2. Effect of the inertia moment of VPB on equivalent dynamic elastic moduli

As can be seen from Fig. 6(b), concentrated inertia moment I representing the VPB is applied on joints, whereas I_α is the inertia moment of the inclined UCE with length l . An inspection on Eq. (5) indicates that the inertia moment of VPB I only affects $K_{66}^{OA}(\omega)$ and $K_{66}^{OC}(\omega)$, and subsequently $G_{12}(\omega)$. It is therefore expected that I affect the equivalent $G_{12}(\omega)$ only. This is evidently in Fig. 8.

Moreover, the effect of I on $G_{12}(\omega)$ is relatively large at 0–0.1 I/I_α , while the trend becomes stable once greater than 0.1 I/I_α . When $\omega/\omega_0 > 50$, $G_{12}(\omega)$ changes monotonically with the increase of I . It

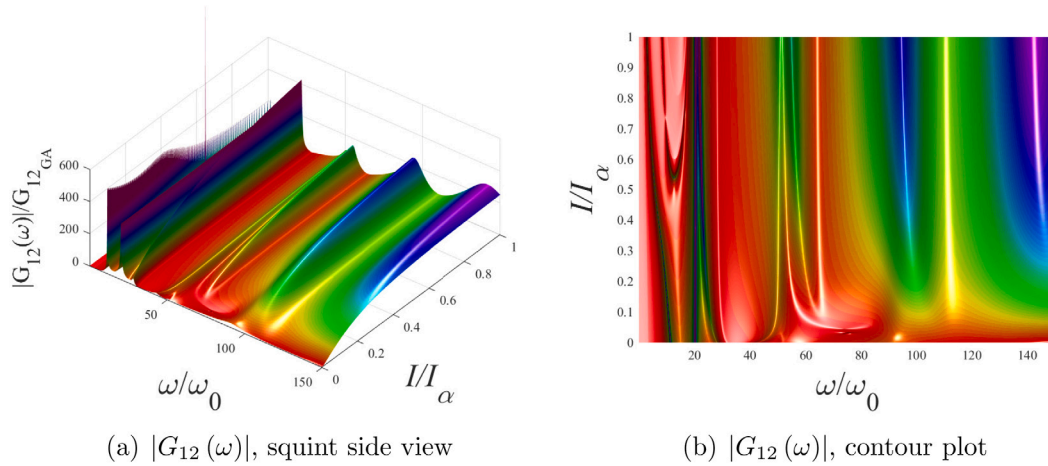


Fig. 8. The equivalent dynamic shear modulus $G_{12}(\omega)$ is normalized with respect to its corresponding static shear modulus in Eq. (36). Absolute value of the results are plotted as functions of the normalized frequency ω/ω_0 and I/I_α .

Table 1

The dependency of the dynamic elastic moduli on m , I and r/l (size), as well as the interpretations from mathematical and physical aspects.

		m	I	r/l
Dependency	E_1, ν_{12}	◆◆	N/A	◆◆
N/A: irrelevant	E_2, ν_{21}	◆◆	N/A	◆◆
◆: weak, ◆◆: strong	G_{12}	◆	◆◆	◆◆
Mathematical interpretation	E_1, ν_{12}	$m \rightarrow K_{44}^{OA}, K_{55}^{OA} \rightarrow E_1, \nu_{12}$	N/A	
	E_2, ν_{21}	$m \rightarrow K_{44}^{OA}, K_{44}^{OC}, K_{55}^{OA} \rightarrow E_2, \nu_{21}$	N/A	$r/l \rightarrow \bar{h}, \bar{l} \rightarrow K_{ij}^{OA}, K_{ij}^{OC} \rightarrow E_1, E_2, \nu_{12}, \nu_{21}, G_{12}$
	G_{12}	$m \rightarrow K_{55}^{OC} \rightarrow G_{12}$	$I \rightarrow K_{66}^{OA}, K_{66}^{OC}, K_{33}^{OA} \rightarrow G_{12}$	
Physical interpretation		Translational inertia	Rotational inertia	Stiffness caused by VPB

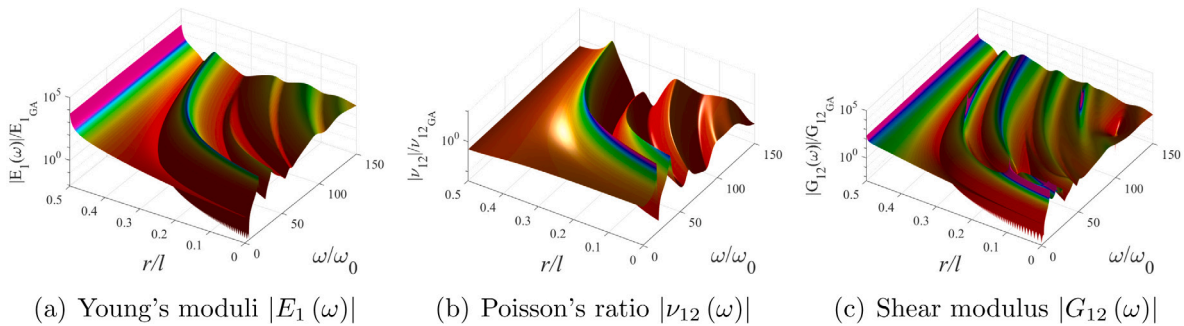


Fig. 9. The equivalent dynamic elastic moduli are normalized with respect to their corresponding static elastic moduli in Eqs. (32), (34) and (36). Absolute value of the results are plotted as functions of the normalized frequency ω/ω_0 and r/l . Here $t/l = 0.1$, $h/l = 1$ and $\theta = \pi/6$.

can be seen that the influence mechanism of I is very similar to that of m .

4.3. Effect of size (stiffness) of VPB on equivalent dynamic elastic moduli

In Fig. 6(c), the massless circular stiffened joints (without m and I) is rigidly connected to UCes. As a result, the presence of the circular stiffened joints increase the ‘stiffness’ of the lattice structures as the radius of the joints increases. The absolute value of equivalent dynamic elastic moduli are plotted as 3D surface plot with respect to ω/ω_0 and r/l in Fig. 9.

It can be seen from Fig. 9 that, the size of the stiffened joints (r/l) affect the dynamic elastic moduli significantly. The size of the stiffened joints has much greater effect on dynamic elastic moduli compared with the influence of m or I . The larger size of the stiffened joints, the fewer the resonance and anti-resonance points occur with ω/ω_0 until the dynamic elastic moduli is no longer affected by ω/ω_0 . That is, the resonance/anti-resonance points move to higher frequency.

In addition, we explored the effect of the size (stiffness) of the circular stiffened joints on static equivalent elastic moduli of the lattice structures as shown in Fig. 10. The static equivalent Young’s moduli and shear modulus increase with the increment of rigid joint size. The positive Poisson’s ratio decreases as rigid joint size becomes larger, while the negative Poisson’s ratio decreases with the increase of the rigid joint size (i.e. the transverse deformation becomes smaller).

In summary, we have obtained three different effects of VPB on the equivalent dynamic elastic moduli. In order to have a more clear and direct understanding of the influence mechanism, Table 1 summarizes the roles played by m , I and size (stiffness) of VPB, companied by the interpretation from mathematical and physical aspects.

5. Equivalent dynamic elastic moduli of four different types of lattice structures with Plateau borders

The roles played by mass, the inertia moment and size (stiffness) of VPB has been investigated and interpreted in Section 4. Our model

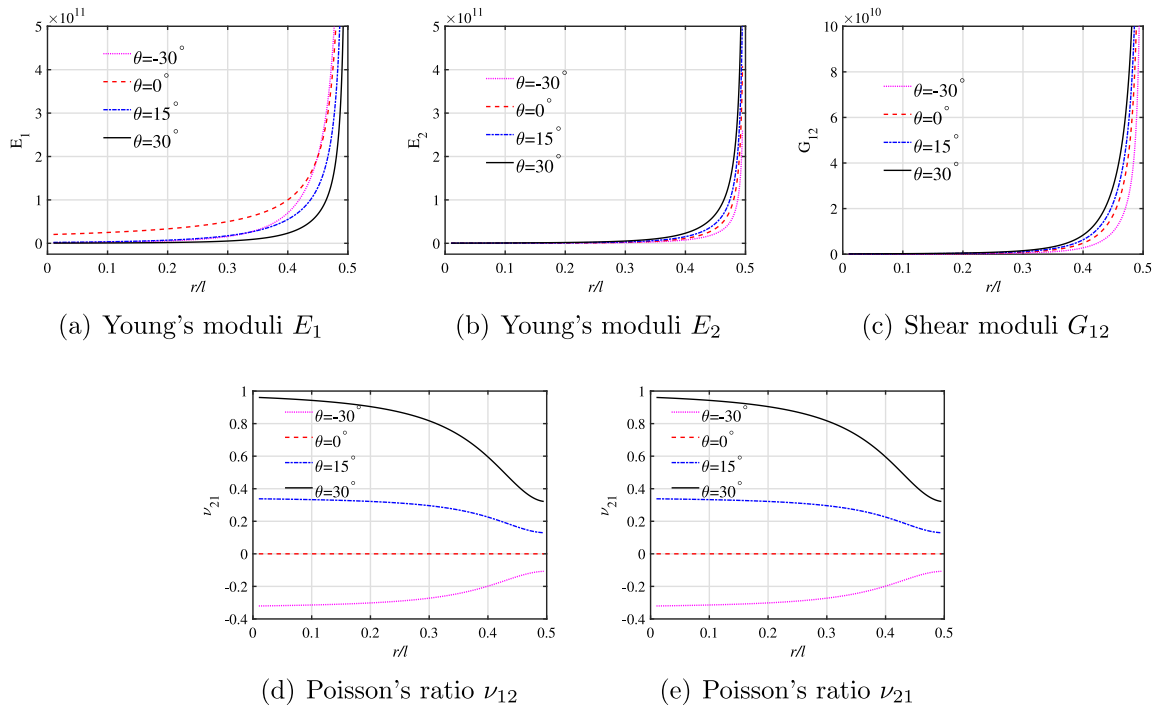


Fig. 10. The equivalent elastic moduli using static Timoshenko beam theory. The results are plotted as functions of r/l for different θ . Here $t/l = 0.1$, $h/l = 1$.

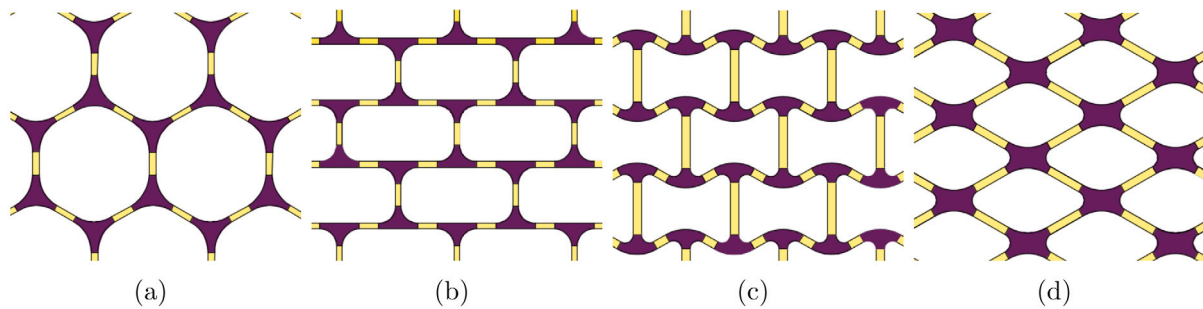


Fig. 11. (a) Hexagonal lattice structure ($\theta > 0$) with Plateau borders. (b) Rectangular lattice structure ($\theta = 0$) with Plateau borders. (c) Auxetic lattice structure ($\theta < 0$) with Plateau borders. (d) Rhombus lattice structure ($\theta = 0$) with Plateau borders.

can cover four types of lattice structures as shown in Fig. 11(a)–(d) by varying θ , h/l and shape of VPB. In what follows, we discuss the roles played by VPB on the equivalent dynamic elastic moduli of those four types of lattice structures.

5.1. Hexagonal honeycomb lattice structures ($\theta > 0$) with Plateau borders

Hexagonal honeycomb lattice structure is one of the most common lattice structures in nature and engineering. As shown in Fig. 11(a), the dark parts correspond to VPBs, while the pale yellow parts correspond to UCes. Here $\theta = 30^\circ$, $h/l = 1$, $r_1 = r_2 = r$. Assuming that the density of VPBs ρ is equal to that of UCes ρ_b , the equivalent dynamic elastic moduli of the hexagonal honeycomb lattice structure with Plateau borders is first explored by varying r/l , as shown in Fig. 12(a–c).

As can be seen from Fig. 12, as the size of the VPB increases, the resonant/anti-resonance points of the plots shift toward higher frequency. Considering the existence of m and I , the resonant/anti-resonance points are less than that in Fig. 9. These conclusions agree well with the physical interpretation summarized in Table 1.

Suppose $\rho = 5\rho_b$, the results in Fig. 13 are different from that in Fig. 12. Increased ρ leads to larger m . It can be found $E_1(\omega)$ and $G_{12}(\omega)$ become larger while $\nu_{12}(\omega)$ becomes smaller. Fewer resonant/anti-resonance points shift to higher frequency, which is similar to the results in Fig. 7.

Next, we explore the effect of θ on the equivalent dynamic elastic moduli as shown in Fig. 14, where the lattice is hexagonal and θ is positive. Here $\rho = \rho_b$, $h/l = 1$, $\bar{h}/h = \bar{l}/l = 0.4$.

The equivalent dynamic elastic moduli of the hexagonal honeycomb lattice structures with Plateau borders for different θ are plotted in Fig. 14(a), which are compared with those for the hexagonal honeycomb lattice structures without Plateau borders plotted in Fig. 14(b). By comparing the above conditions, it can be found the number of resonant/anti-resonance points is less due to the presence of VPB.

When $h/l \neq 1$, the equivalent dynamic elastic moduli will also change significantly. Here $\theta = \pi/6$, $r/l = 0.3$, $l = 1$ and $h/l \in (1, 10)$. The equivalent dynamic elastic moduli with change of h/l is studied in Figs. 15(a–b) and 16.

As can be seen from Fig. 15, dynamic elastic moduli in direction-1 is less affected by h/l . We assume that $l = 1$ and h is varying. $E_1(\omega)$ and

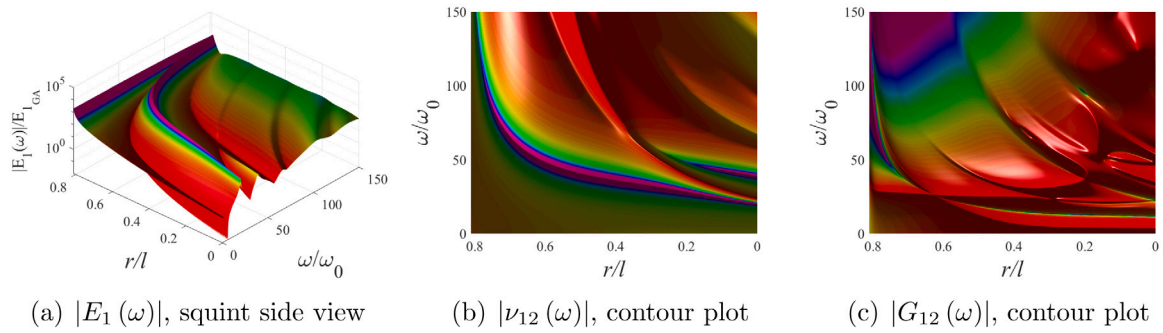


Fig. 12. The equivalent dynamic elastic moduli are normalized with respect to their corresponding static elastic moduli in Eqs. (32), (34) and (36). Absolute value of the results are plotted as functions of the normalized frequency ω/ω_0 and r/l . Here $\rho = \rho_b$ (the density of the VPB and UCE are the same), $\theta = 30^\circ$, $h/l = 1$.

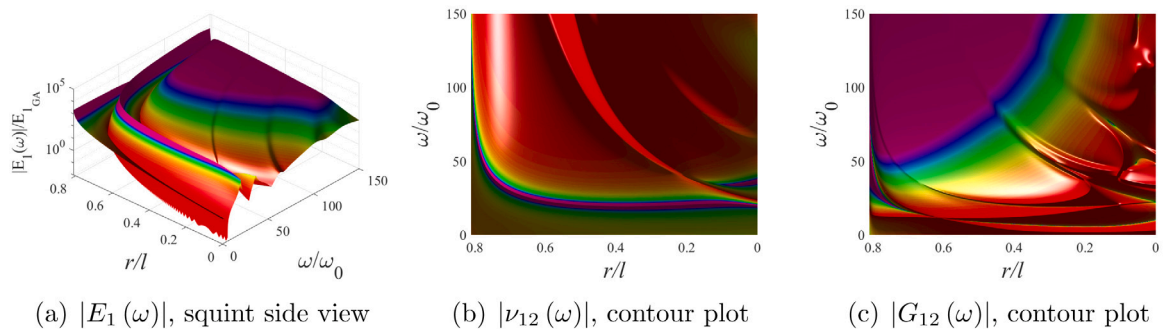
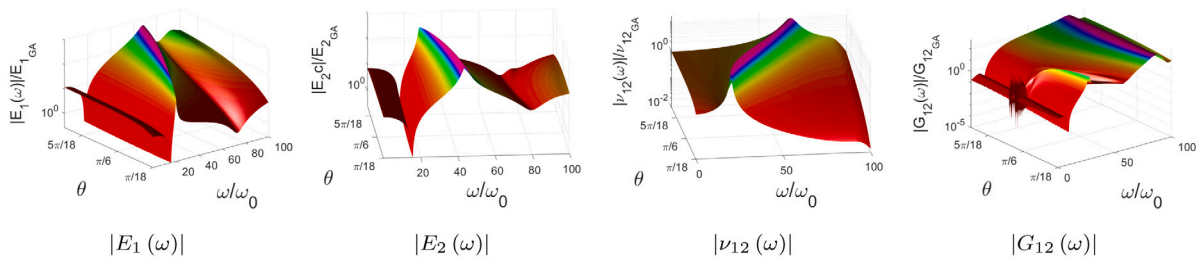
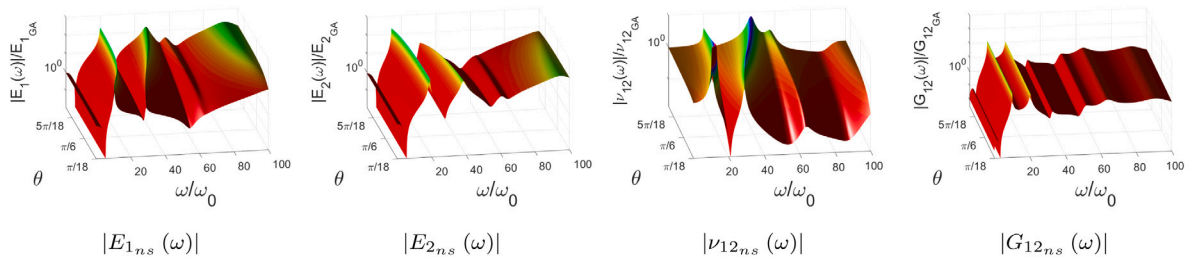


Fig. 13. The same as for Fig. 12 except that $\rho = 5\rho_b$, i.e. the density of the VPB is five times of the UCE.



(a) The equivalent dynamic elastic moduli of hexagonal lattice structure with Plateau borders.



(b) The equivalent dynamic elastic moduli of hexagonal lattice structure without Plateau borders.

Fig. 14. The equivalent dynamic elastic moduli are normalized with respect to their corresponding static elastic moduli in Eqs. (32)–(36). Absolute value of the results are plotted as functions of the normalized frequency ω/ω_0 and θ .

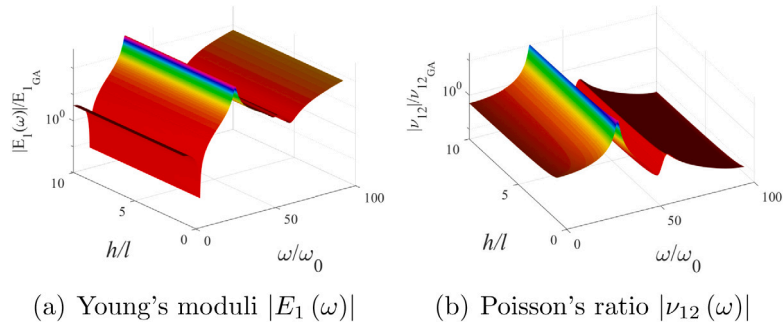
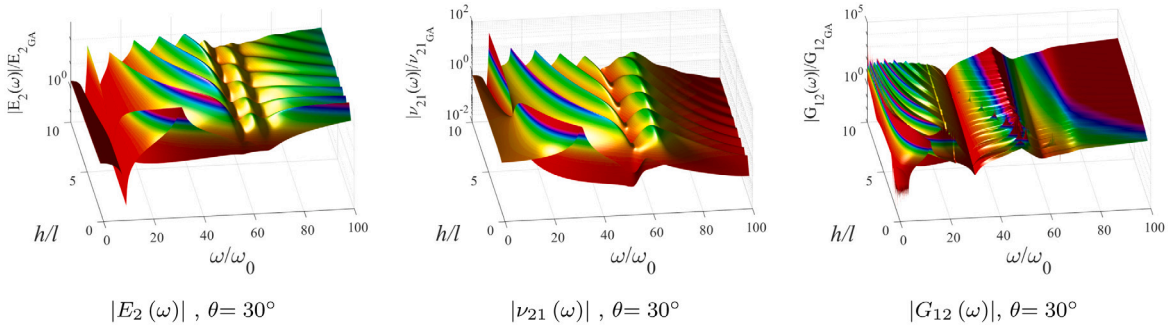
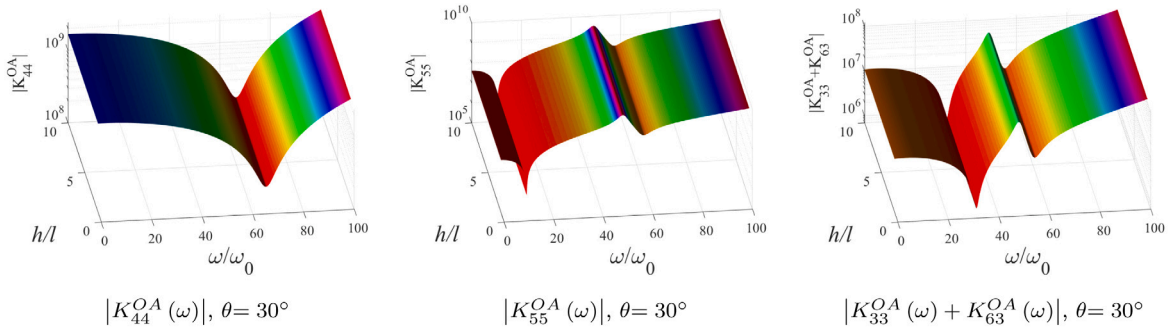


Fig. 15. The equivalent dynamic elastic moduli($E_1(\omega)$, $\nu_{12}(\omega)$) are normalized with respect to their corresponding static elastic moduli in Eqs. (32) and (34). Absolute value of the results are plotted as functions of the normalized frequency ω/ω_0 and h/l . Here $\theta = \pi/6, r/l = 0.3, l = 1$.



(a) The equivalent dynamic elastic moduli are normalized with respect to their corresponding static elastic moduli in Eqs. (33), (35) and (36).



(b) The dynamic stiffness coefficients of inclined members $K_{44}^{OA}(\omega)$, $K_{55}^{OA}(\omega)$ and $K_{33}^{OA}(\omega) + K_{63}^{OA}(\omega)$. These coefficients lead to the unchanged resonant/anti-resonance points in Fig. 16(a).

Fig. 16. Absolute value of the equivalent dynamic elastic moduli and dynamic stiffness coefficients are plotted as functions of the normalized frequency ω/ω_0 and h/l . Here $\theta = \pi/6, r/l = 0.3, l = 1$.

$\nu_{12}(\omega)$ is mainly influenced by the deformation of the inclined members. The dynamic stiffness coefficients of vertical members (i.e. K_{ij}^{OC}) did not affect $E_1(\omega)$ and $\nu_{12}(\omega)$ from Eqs. (9)–(11).

However, the effect on the dynamic elastic moduli in direction-2 is relatively significant in Fig. 16(a). As h/l increases, the resonant/anti-resonance points move to the lower frequency due to the smaller size of VPB. Besides, the local maximum/minimum of $K_{44}^{OA}(\omega)$, $K_{55}^{OA}(\omega)$ and $K_{33}^{OA}(\omega) + K_{63}^{OA}(\omega)$ are not affected by h from Fig. 16(b). These values lead to the unchanged resonant/anti-resonance points of dynamic elastic moduli in direction-2.

5.2. The rectangle lattice ($\theta = 0^\circ$) with Plateau border

Based on the unit cell in this paper, if $\theta = 0^\circ$, then the rectangular lattice structure [70,71] is obtained. The equivalent dynamic elastic

moduli can be expressed as

$$E_1(\omega) = \frac{K_{44}^{OA}(\omega)}{b}, E_2(\omega) = \frac{K_{55}^{OA}(\omega)}{b \left(1 + 2 \frac{K_{55}^{OA}(\omega)}{K_{44}^{OA}(\omega)} \right)} \quad (40)$$

$$\nu_{12}(\omega) = \nu_{21}(\omega) = 0 \quad (41)$$

$$G_{12}(\omega) = \frac{1}{b \left(\frac{2K_{66}^{OC}(\omega) + hK_{56}^{OC}(\omega)}{K_{55}^{OC}(\omega)K_{66}^{OC}(\omega) - (K_{56}^{OC}(\omega))^2} + \frac{(K_{66}^{OA}(\omega) - K_{36}^{OA}(\omega))h^2}{2(K_{33}^{OA}(\omega)K_{66}^{OA}(\omega) - K_{36}^{OA}(\omega)K_{63}^{OA}(\omega))} \right)} \quad (42)$$

In Eq. (41), the Poisson's ratios are 0. Thus, we only explore the Young's moduli and shear modulus. The rectangular lattice structure

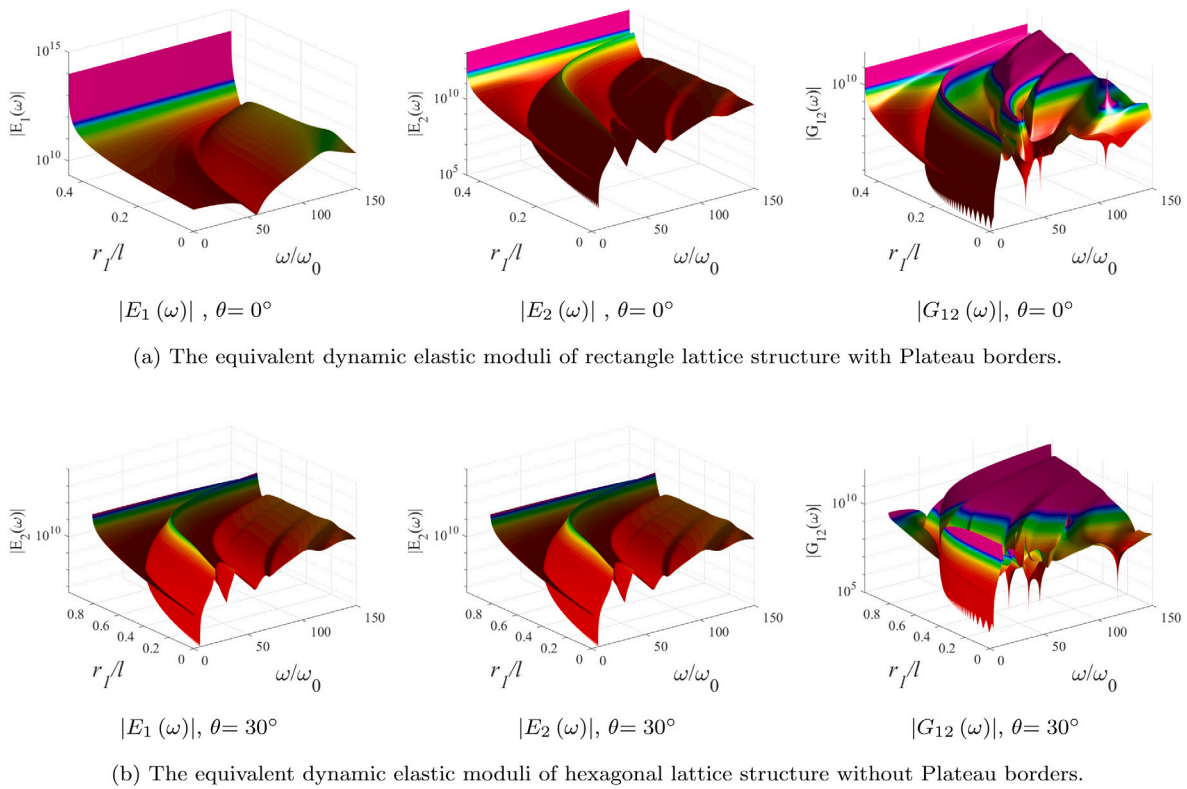


Fig. 17. Absolute value of equivalent dynamic elastic moduli is plotted as functions of the normalized frequency ω/ω_0 and r_1/l .

with Plateau borders is shown in Fig. 11(b). Here $\rho = \rho_b$. To make a comparison, we explore the equivalent dynamic elastic moduli of the rectangular lattice and hexagonal lattice as r_1/l changes in Fig. 17, respectively.

Compared with the results in Fig. 17(a), we can draw the following conclusions on the rectangle lattice from Fig. 17(b): (1) The upper and lower magnitude limits of the equivalent dynamic elastic moduli of rectangle lattice structure with Plateau borders are larger than that of hexagonal lattice structure with Plateau borders. (2) The resonant/anti-resonance points of $E_1(\omega)$ of rectangle lattice structure with Plateau borders are less than that of hexagonal lattice structure with Plateau borders, as a result of which the deformation in direction-1 is only dominated by stretching ($K_{44}^{OA}(\omega)$). However, because the deformation in direction-2 is still dominated by stretching and bending ($K_{44}^{OC}(\omega)$ and $K_{55}^{OA}(\omega)$), the change of resonant/anti-resonance points of $E_2(\omega)$ is not obvious.

5.3. Auxetic lattice structure ($\theta < 0$) with Plateau borders

The schematic diagram of auxetic lattice structure [72,73] with Plateau borders is shown in Fig. 11(c). The important feature of auxetic lattice structure is the negative Poisson's ratio [72,74–76]. Since damping is taken into account, the equivalent dynamic elastic moduli are complex values. Therefore, in addition to analysing the absolute value of equivalent dynamic elastic moduli, the real part of Poisson's ratio is also studied. Here $\rho = \rho_b$, $h/l = 2$, $\bar{h}/h = \bar{l}/l = 0.4$.

The equivalent dynamic elastic moduli of the auxetic lattice with Plateau borders for different θ are plotted in Fig. 18(a), which are compared with those for the auxetic lattice without Plateau borders plotted in Fig. 18(b). Similar conclusions can be drawn from Fig. 18 with those from Fig. 14. Besides, different θ leads to different shapes and therefore different m of VPB, especially for $\theta < 0$. For example, when $\theta \in (-\frac{\pi}{9}, -\frac{5\pi}{18})$, the effect of θ on resonant/anti-resonance points is very obvious as shown in Fig. 18(a).

5.4. Rhombus lattice ($\bar{h} = 0$) with Plateau borders

If we take $\bar{h} = 0$ from the unit cell model considered in this paper, it becomes rhombus lattice structure with Plateau borders as illustrated in Fig. 11(d). Therefore, we have

$$E_1(\omega) = \frac{K_{44}^{OA}(\omega)}{b \sin \theta \cos \theta \left(1 + \tan^2 \theta \frac{K_{44}^{OA}(\omega)}{K_{55}^{OA}(\omega)} \right)},$$

$$E_2(\omega) = \frac{K_{55}^{OA}(\omega) \sin \theta}{b \cos^3 \theta \left(1 + \tan^2 \theta \frac{K_{55}^{OA}(\omega)}{K_{44}^{OA}(\omega)} \right)}, G_{12}(\omega) = \frac{\tan \theta}{b} \quad (43)$$

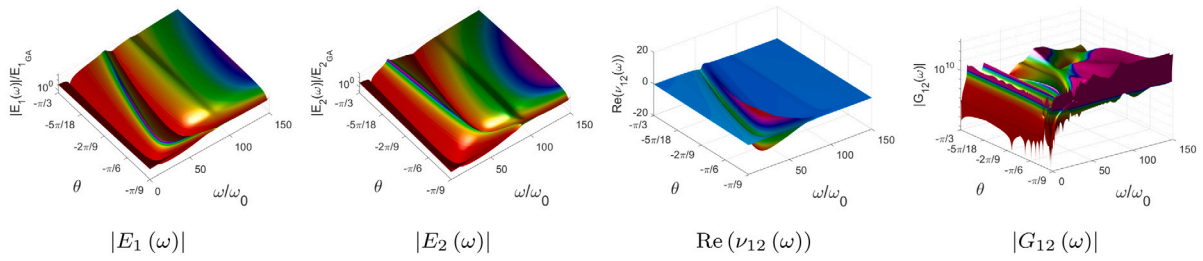
$$v_{12}(\omega) = \frac{\frac{K_{44}^{OA}(\omega)}{K_{55}^{OA}(\omega)} - 1}{\tan^2 \theta \frac{K_{44}^{OA}(\omega)}{K_{55}^{OA}(\omega)} + 1}, v_{21}(\omega) = \frac{\sin^2 \theta \left(1 - \frac{K_{55}^{OA}(\omega)}{K_{44}^{OA}(\omega)} \right)}{\cos^2 \theta \left(1 + \tan^2 \theta \frac{K_{55}^{OA}(\omega)}{K_{44}^{OA}(\omega)} \right)} \quad (44)$$

It is clear from Eqs. (43) that the shear modulus G_{12} is independent of frequency.

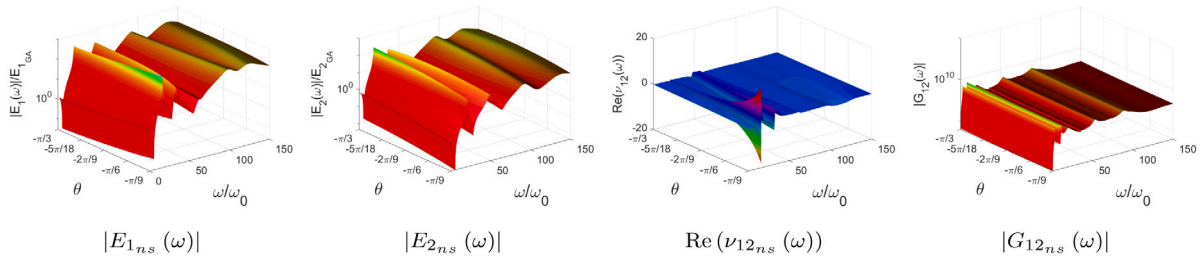
Here, $\rho = \rho_b$ (the density of the VPB and UCE are the same). The geometric parameters of the rhombus lattice with Plateau borders are taken as: $h/l = 1, \bar{h}/h = 0, \bar{l}/l = 0.4$, while that of the hexagonal honeycomb structure with Plateau borders are: $h/l = 1, \bar{h}/h = \bar{l}/l = 0.4$. Their dynamic elastic moduli for different θ are plotted in Fig. 19(a) and (b), respectively. By comparing the results of Figs. 19(a) and (b), the change of the dynamic elastic moduli for different θ is small. This is because the deformation of the vertical members has a smaller weight than that of the inclined members.

6. Conclusion

A general analytical framework is presented for the broadband equivalent dynamic elastic moduli of lattice structures with Plateau

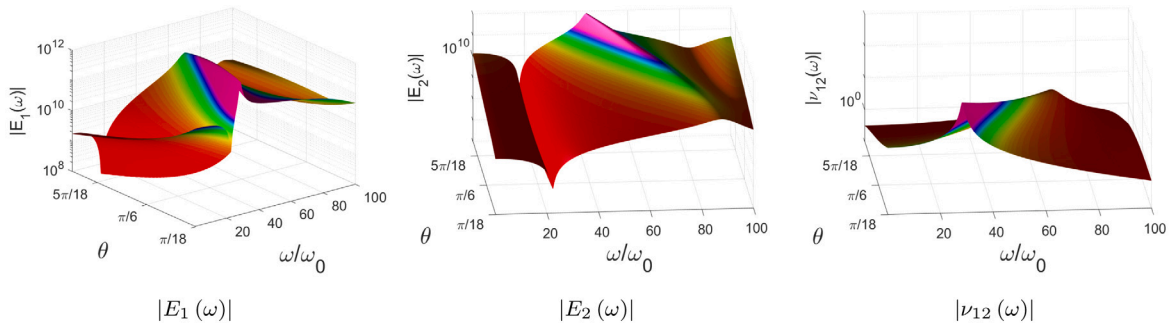


(a) The equivalent dynamic elastic moduli of the auxetic lattice with Plateau borders.



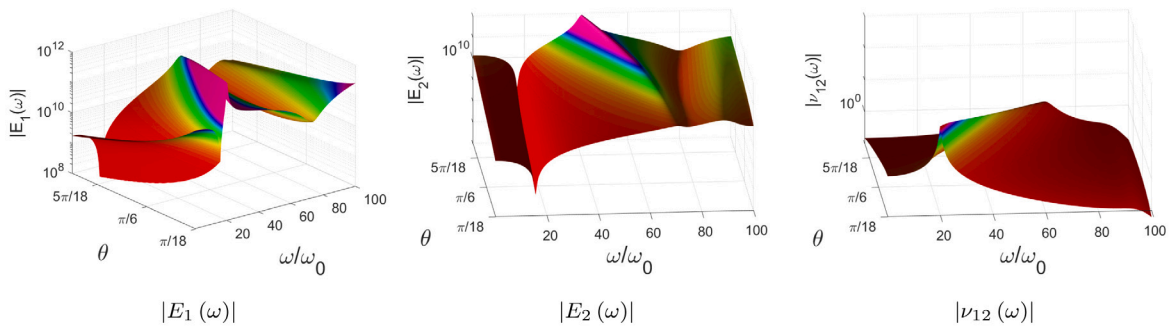
(b) The equivalent dynamic elastic moduli of the auxetic lattice without Plateau borders.

Fig. 18. Absolute value of equivalent dynamic elastic moduli and real part of $\nu_{12}(\omega)$ are plotted as functions of the normalized frequency ω/ω_0 and θ .



(a) The equivalent dynamic elastic moduli of rhombus lattice structure with Plateau borders. Here

$$h/l = 1, \bar{h}/h = 0, \bar{l}/l = 0.4.$$



(b) The equivalent dynamic elastic moduli of hexagonal lattice structure with Plateau borders. Here

$$h/l = 1, \bar{h}/h = \bar{l}/l = 0.4$$

Fig. 19. Absolute value of equivalent elastic moduli is plotted as functions of the normalized frequency ω/ω_0 and θ .

borders under steady-state conditions. Key novel features of this paper include:

(1) First, the analytical dynamic stiffness formulation of a unit cell of lattice structures with Plateau borders is developed. For the unit cell, the flexible cell edge is modelled by the exact beam DS formulations

based on rod and Timoshenko theories, whereas the vertexes with Plateau borders (VPBs) are modelled by rigid bodies with mass, inertia moment and size properties. The DS formulations of both the flexible cell edge and VPB are assembled for the unit cell according to rigid body dynamics.

(2) Then, the analytical expressions of equivalent dynamic elastic moduli are proposed by applying the associate boundary conditions. In particular, the equivalent shear modulus is developed based on a novel but more reasonable unit cell.

(3) Based on the above analytical expressions, investigations reveal that the VPBs exert significant influence on the equivalent dynamic elastic moduli of lattice structures. It is found that Young's moduli E_1 and E_2 and Poisson's ratio ν_{12} and ν_{21} are obviously affected by the VPB mass, whereas the shear modulus G_{12} is mainly affected by the moment of inertia of the VPB as expected. Moreover, all dynamic elastic moduli are influenced by the VPB size (stiffness). Related physical and mathematical interpretations are provided.

(4) Besides, the present framework is sufficient general to be applied to a wide range of lattice structures with Plateau borders, such as, honeycomb, rectangular, auxetic and rhombic lattice structures. Physical and mathematical insights on the effects of the VPB on the dynamic elastic moduli have been gained due to the analytical essence of this work.

This work not only provides analytical expressions of frequency-dependent equivalent dynamic elastic moduli for the dynamic analysis of structures composed of lattice structures with VPB, but also sheds lights on the enhancement design of lattice structures by taking advantage of VPB. It also proposed a general analytical framework for the dynamic homogenization of lattice structures with imperfections. Extensions of the current research include, but not limited to, the equivalent dynamic moduli of different types of 2D or 3D lattice structures with different shapes of stiffened vertex and their applications to the broadband dynamic analysis of lattice-core panels.

CRedit authorship contribution statement

X. Liu: Conceptualization, Methodology, Writing – review & editing, Supervision, Project administration, Funding acquisition. **L. Huang:** Investigation, Data curation, Writing – original draft, Writing – review & editing. **S. Adhikari:** Writing – review & editing.

Data availability

No data was used for the research described in the article.

Acknowledgements

The authors appreciate the financial supports from the National Natural Science Foundation of China (Grant No. 11802345), State Key Laboratory of High Performance Complex Manufacturing, China (Grant No. ZZYJKT2019-07), Central South University, China (Grant No. 502045001) and the High-end foreign expert introduction project, China through Grant no G20190018004 which made this research possible.

Appendix A. Axial vibration based on classical rod theory

According to classical rod theory, the equation governing axial motion of a damped beam is [77,78]

$$EA \left(1 + \zeta_k \frac{\partial}{\partial t}\right) \frac{\partial^2 u}{\partial x^2} - \rho A \frac{\partial^2 u}{\partial t^2} - c_a \frac{\partial u}{\partial t} = 0 \tag{A.1}$$

where EA is the stiffness of axial deformation, ρA is the mass per unit length, ζ_k is the stiffness damping factor of stiffness, and c_a is the velocity-dependent viscous damping coefficient. According to the derivation process of [47], the specific expressions of a_1 and a_2 in the matrix can be obtained

$$a_1 = \frac{EA(1 + i\omega\zeta_k)k_1}{\bar{l}} \cot(k_1), a_2 = -\frac{EA(1 + i\omega\zeta_k)k_1}{\bar{l}} \csc(k_1) \tag{A.2}$$

where

$$k_1^2 = \frac{(\rho A\omega^2 - i\omega c_a)\bar{l}^2}{EA(1 + i\zeta_k\omega)} \tag{A.3}$$

Appendix B. Bending vibration based on Timoshenko beam theory

According to Timoshenko beam theory, the governing differential equation for bending vibration is given as follows [77]

$$kAG \left(1 + \zeta_k \frac{\partial}{\partial t}\right) \frac{\partial}{\partial x} \left(\frac{\partial \omega}{\partial x} - \theta\right) - \rho A \frac{\partial^2 \omega}{\partial t^2} - c_s \frac{\partial \omega}{\partial t} = 0 \tag{B.1}$$

$$EI \left(1 + \zeta_k \frac{\partial}{\partial t}\right) \frac{\partial^2 \theta}{\partial x^2} + kAG \left(1 + \zeta_k \frac{\partial}{\partial t}\right) \left(\frac{\partial \omega}{\partial x} - \theta\right) - \rho I \frac{\partial^2 \theta}{\partial t^2} - c_b \frac{\partial \theta}{\partial t} = 0 \tag{B.2}$$

where EI is the bending stiffness of the beam, I is the inertia moment of the beam, ρ is the density of the beam, A is the cross-section area of the beam, then ρA is the mass per unit length of the beam, kAG is the shear stiffness of the beam, k is the shear correction value (also known as the shape function), and c_s and c_b are the velocity-dependent viscous damping coefficients of shear and bending deformation. The amplitudes of shear force and bending moment are given by the following equations

$$V(x) = -kAG \left(\frac{\partial \omega}{\partial x} - \theta\right) = EI \frac{\partial^2 \theta}{\partial x^2} + \rho I \omega^2 \theta \tag{B.3}$$

$$M(x) = -EI \frac{\partial \theta}{\partial x} \tag{B.4}$$

Then we can get

$$\begin{aligned} d_1 &= R_3 \bar{b}^{-2} \alpha (cS + \eta_2 sC) / (k_1 k_2) \\ d_2 &= R_2 \alpha \lambda_1 [(k_1 + \eta_1 k_2) sS - (k_2 - \eta_2 k_1) (1 - cC)] / (k_2 + \eta_2 k_1) \\ d_3 &= R_1 \alpha (sC - \eta_1 cS) \\ d_4 &= -R_3 \bar{b}^{-2} \alpha (S + \eta_2 s) / (k_1 k_2) \\ d_5 &= R_2 \alpha \lambda_1 (C - c) \\ d_6 &= R_1 \alpha (\eta_1 S - s) \end{aligned} \tag{B.5}$$

where

$$\begin{aligned} \alpha &= \frac{k_2 + \eta_2 k_1}{2\eta_2(1 - cC) + (1 - \eta_1^2) sS}, \eta_1 = \frac{\lambda_1}{\lambda_2}, \eta_2 = j \frac{\lambda_1}{\lambda_2} \\ R_i &= \frac{(1 + i\omega\zeta_k)EI}{\bar{l}^i}, \begin{bmatrix} s \\ c \end{bmatrix} = \begin{bmatrix} \sin k_1 \\ \cos k_1 \end{bmatrix} \\ \begin{bmatrix} S \\ C \end{bmatrix} &= \begin{bmatrix} \sinh k_2 \\ \cosh k_2 \end{bmatrix}, \text{ for } \bar{b}^{-2} r^2 s^2 < 1 \\ \begin{bmatrix} S \\ C \end{bmatrix} &= \begin{bmatrix} \sin k_2 \\ \cos k_2 \end{bmatrix}, \text{ for } \bar{b}^{-2} r^2 s^2 > 1 \\ \lambda_1 &= \frac{k_1^2 - \bar{b}^{-2} s^2}{2}, \lambda_2 = \frac{k_2^2 + j\bar{b}^{-2} s^2}{2} \\ k_1^2 &= \frac{\bar{b}^{-2}(r^2 + s^2)}{2} + \frac{\bar{b}^{-2}}{2} \sqrt{(r^2 + s^2)^2 + \frac{4}{\bar{b}^2} (1 - \bar{b}^{-2} r^2 s^2)} \\ k_2^2 &= \frac{-\bar{b}^{-2}(r^2 + s^2) + \bar{b}^{-2} \sqrt{(r^2 + s^2)^2 + \frac{4}{\bar{b}^2} (1 - \bar{b}^{-2} r^2 s^2)}}{j} \\ \bar{b}^{-2} &= \frac{(\rho A\omega^2 - i\omega c_s)\bar{l}^4}{EI(1 + i\omega\zeta_k)}, r^2 = \frac{\rho I\omega^2 - i\omega c_b}{(\rho A\omega^2 - i\omega c_s)\bar{l}^2}, s^2 = \frac{EI}{kAG\bar{l}^2} \end{aligned} \tag{B.6}$$

Appendix C. The unit cell model and expression of $G_{12}(\omega)$ in [47]

To illustrate the difference of derivation of $G_{12}(\omega)$ between this paper and [47], unit cell model and expression of $G_{12}(\omega)$ in [47] are provided as follows.

See Fig. C.1

$$G_{12}(\omega) = \frac{(\beta + \sin \theta)}{b \cos \theta} \frac{1}{\left(-\frac{h^2}{2lK_{55}(\omega)} + \frac{4K_{66}^{(h/2)}(\omega)}{\left(K_{55}^{(h/2)}(\omega)K_{66}^{(h/2)}(\omega) - \left(K_{56}^{(h/2)}(\omega) \right)^2 \right)} + \frac{(\cos \theta + (h/l + \sin \theta) \tan \theta)^2}{K_{44}(\omega)} \right)} \tag{C.1}$$

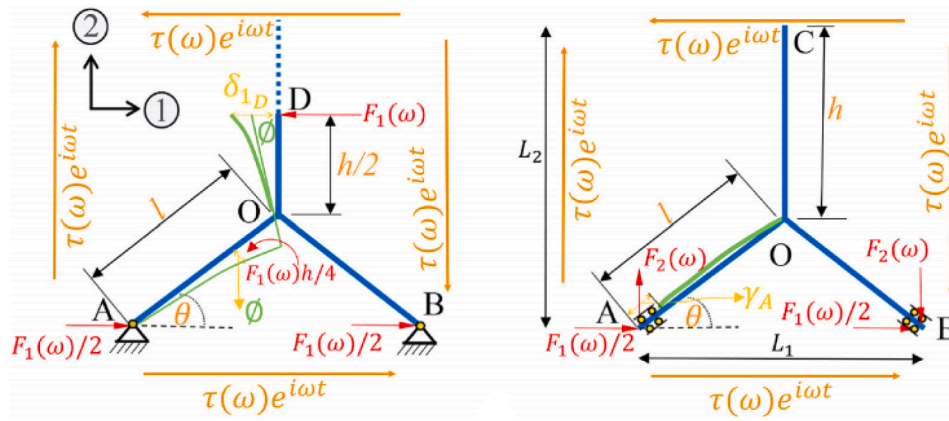


Fig. C.1. Two separate unit cells are used for deriving the in-plane shear modulus in [47].

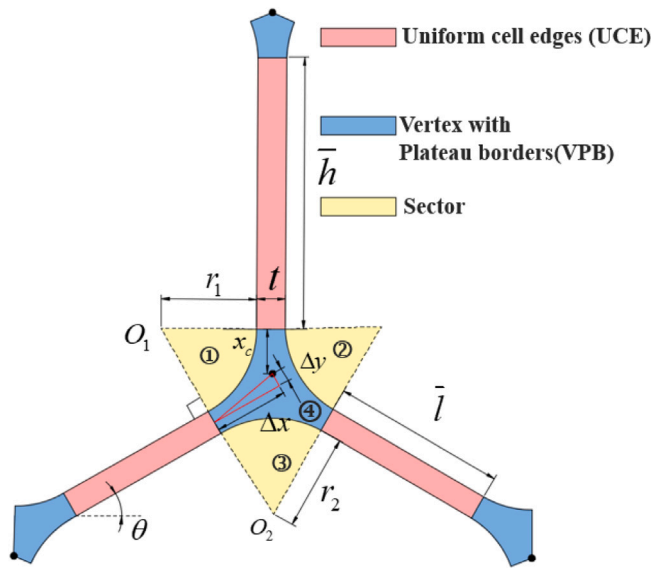


Fig. D.2. Unit cell of lattice structures with Plateau borders.

Appendix D. Geometric and physical parameters of the vertexes with plateau border (VPB)

When analysing the equivalent dynamic elastic moduli of different types of lattice structures with Plateau borders, we need to know geometric and physical parameters of VPB such as the mass, the inertia moment, and the distance between the mass centre of VPB to the centre of the rigid connection. Thus, we give the derivation procedure for these parameters of the typical honeycomb lattice structures with Plateau borders as follows. As can be seen from Fig. D.2, supposing the O_1O_2 is perpendicular to the inclined uniform cell edge (UCE), we have

$$r_2 = \frac{c}{\sin \theta} - r_1 - t \quad (D.1)$$

where

$$c = r_1 + t/2 \quad (D.2)$$

Then we find out the centres of sector ①, ②, ③ and triangles composed of ①, ②, ③ and VPB ④. Finally, the centre of VPB ④ can be obtained by overlap method

$$x_c = \frac{6c\theta r_2^2 \cot \theta - 2c^3 \cot^2 \theta - 4r_2^3 \sin \theta + 8r_1^3 \sin^2(\theta/2 - \pi/4)}{3(-2\theta r_1^2 + \pi r_1^2 + 2\theta r_2^2 - 2c^2 \cot \theta)} \quad (D.3)$$

Then, according to geometrical relationships, the distance between the mass centre of VPB to the centre of the rigid connection in the direction of inclined UCE is obtained

$$\Delta x = (1 + \sin \theta)x_1 - x_c \sin \theta \quad (D.4)$$

The distance in the direction perpendicular to the inclined UCE is

$$\Delta y = (x_1 - x_c) \cos \theta \quad (D.5)$$

where

$$x_1 = (r_1 + t/2) \tan(\pi/4 - \theta/2) \quad (D.6)$$

The distance between the mass centre of VPB to the centre of the rigid connection in the direction of vertical member is

$$\Delta x_h = x_c \quad (D.7)$$

The distance in the direction perpendicular to the vertical member is

$$\Delta y_h = 0 \quad (D.8)$$

The mass of VPB can be obtained through multiplying the area of Plateau borders by height b and then multiplying the density ρ , whereas the inertia moment of VPB is also based on superposition method and parallel axis theorem. Moreover, the derivation method for the geometric and physical parameters of other types of lattice structures with Plateau borders is similar but is not repeated here.

References

- [1] Dharmasena KP, Wadley HNG, Xue Z, Hutchinson JW. Mechanical response of metallic honeycomb sandwich panel structures to high-intensity dynamic loading. *Int J Impact Eng* 2008;35:1063–74.
- [2] Song J, Zhou W, Wang Y, Fan R, Wang Y, Chen J, Lu Y, Li L. Octet-truss cellular materials for improved mechanical properties and specific energy absorption. *Mater Des* 2019;173:107773.
- [3] Li W, Fan H, Bian Y, Yang F. Plastic deformation and energy absorption of polycrystalline-like lattice structures. *Mater Des* 2021;198:109321.
- [4] Yungwirth CJ, Radford DD, Aronson M, Wadley HNG. Experiment assessment of the ballistic response of composite pyramidal lattice truss structures. *Composites B* 2008;39:556–69.
- [5] Zheng J, Zhao L, Fan H. Energy absorption mechanisms of hierarchical woven lattice composites. *Composites B* 2012;43(3):1516–22. <http://dx.doi.org/10.1016/j.compositesb.2011.08.034>.
- [6] Hu J, Zhou J, Zhang A, Yi L, Wang J. Temperature dependent mechanical properties of graphene based carbon honeycombs under tension and compression. *Phys Lett A* 2021;391:127130. <http://dx.doi.org/10.1016/j.physleta.2020.127130>.
- [7] Fabbrocino F, Carpentieri G. Three-dimensional modeling of the wave dynamics of tensegrity lattices. *Compos Struct* 2017;173:9–16. <http://dx.doi.org/10.1016/j.compstruct.2017.03.102>.
- [8] Mancusi G, Fabbrocino F, Feo L, Fraternali F. Size effect and dynamic properties of 2D lattice materials. *Composites B* 2017;112:235–42. <http://dx.doi.org/10.1016/j.compositesb.2016.12.026>.

- [9] Liu X, Lu Z, Adhikari S, Li Y, Banerjee JR. Exact wave propagation analysis of lattice structures based on the dynamic stiffness method and the Wittrick-Williams algorithm. *Mech Syst Signal Process* 2022;174:109044.
- [10] Yahaya MA, Ruan D, Lu G, Dargusch MS. Response of aluminium honeycomb sandwich panels subjected to foam projectile impact: An experimental study. *Int J Impact Eng J* 2015;75:100–9.
- [11] Olympio KR, Gandhi F. Flexible skins for morphing aircraft using cellular honeycomb cores. *J Intell Mater Syst Struct* 2010;21(17):1719–35.
- [12] Davalos JF, Qiao P, Xu XF, Robinson J, Barth KE. Modeling and characterization of fiber-reinforced plastic honeycomb sandwich panels for highway bridge applications. *Compos Struct* 2001;52: 52.
- [13] Yao S, Xiao X, Xu P, Qu Q, Che Q. The impact performance of honeycomb-filled structures under eccentric loading for subway vehicles. *Thin-Walled Struct* 2018;123(October 2017):360–70.
- [14] Mahmoud D, Elbestawi MA. Lattice structures and functionally graded materials applications in additive manufacturing of orthopedic implants: A review. *J Manuf Mater Process Rev* 2017;1–19.
- [15] Zhang Q, Yang X, Li P, Huang G, Lu TJ. Bio-inspired engineering of honeycomb structure - using nature to inspire human innovation. *Prog Mater Sci* 2015;74:332–400.
- [16] Choe J, Huang Q, Yang J, Hu H. An efficient approach to investigate the post-buckling behaviors of sandwich structures. *Compos Struct* 2018;201(June):377–88. <http://dx.doi.org/10.1016/j.compstruct.2018.06.025>.
- [17] Chen TJ, Huang JS. Creep-buckling of hexagonal honeycombs with dual imperfections. *Compos Struct* 2009;89(1):143–50. <http://dx.doi.org/10.1016/j.compstruct.2008.07.018>.
- [18] Restrepo D, Mankame ND, Zavattieri PD. Programmable materials based on periodic cellular solids. Part I: Experiments. *Int J Solids Struct* 2016;100–101:485–504. <http://dx.doi.org/10.1016/j.ijsolstr.2016.09.021>.
- [19] Simone AE, Gibson LJ. Effects of solid distribution on the stiffness and strength of metallic foams. *Acta Mater* 1998;46(6):2139–50.
- [20] Yang MY, Huang JS. Numerical analysis of the stiffness and strength of regular hexagonal honeycombs with plateau borders. *Compos Struct* 2004;64(1):107–14.
- [21] Duan S, Tao Y, Lei H, Wen W, Liang J, Fang D. Enhanced out-of-plane compressive strength and energy absorption of 3D printed square and hexagonal honeycombs with variable-thickness cell edges. *Extrem Mech Lett* 2018;18:9–18.
- [22] Yang MY, Huang JS. Elastic buckling of regular hexagonal honeycombs with plateau borders under biaxial compression. *Compos Struct* 2005;71(2):229–37. <http://dx.doi.org/10.1016/j.compstruct.2004.10.014>.
- [23] Chuang C-h, Huang J-s. Effects of solid distribution on the elastic buckling of honeycombs Cheng-Hsin. *Int J Mech Sci* 2002;44:1429–43.
- [24] Yang MY, Huang JS. Failure surfaces for brittle honeycombs with plateau borders under in-plane biaxial loads. *Compos Struct* 2006;72(4):512–20. <http://dx.doi.org/10.1016/j.compstruct.2005.01.019>.
- [25] Yang MY, Huang JS, Hu JW. Elastic buckling of hexagonal honeycombs with dual imperfections. *Compos Struct* 2008;82(3):326–35.
- [26] Lin TC, Yang MY, Huang JS. Effects of solid distribution on the out-of-plane elastic properties of hexagonal honeycombs. *Compos Struct* 2013;100:436–42.
- [27] Lin JY, Huang JS. Creep of hexagonal honeycombs with Plateau borders. *Compos Struct* 2005;67(4):477–84. <http://dx.doi.org/10.1016/j.compstruct.2004.02.006>.
- [28] Chuang CH, Huang JS. Elastic moduli and plastic collapse strength of hexagonal honeycombs with plateau borders. *Int J Mech Sci* 2002;44(9):1827–44. [http://dx.doi.org/10.1016/S0020-7403\(02\)00139-X](http://dx.doi.org/10.1016/S0020-7403(02)00139-X).
- [29] Zhang K, Deng ZC, Meng JM, Xu XJ. Wave propagation in hexagonal lattices with plateau borders. *Compos Struct* 2016;140:525–33. <http://dx.doi.org/10.1016/j.compstruct.2015.12.046>.
- [30] Meng J, Deng Z, Zhang K, Xu X. Wave propagation in hexagonal and re-entrant lattice structures with cell walls of non-uniform thickness. *Waves Random Complex Media* 2015;25(2):223–42. <http://dx.doi.org/10.1080/17455030.2015.1005195>.
- [31] Amendola A, Fabbrocino F, Feo L, Auricchio F, Fraternali F. Dependence of the mechanical properties of pentamode materials on the lattice microstructure. In: ECCOMAS congress 2016 - Proceedings of the 7th European congress on computational methods in applied sciences and engineering, Vol. 1. 2016, p. 2134–50. <http://dx.doi.org/10.7712/100016.1947.6004>, (January).
- [32] Fabbrocino F, Amendola A, Benzoni G, Fraternali F. Seismic application of pentamode lattices. *Ing Sismica* 2016;33(1–2):62–70.
- [33] Foo CC, Chai GB, Seah LK. Mechanical properties of nomenclature material and nomenclature honeycomb structure. *Compos Struct* 2007;80(4):588–94. <http://dx.doi.org/10.1016/j.compstruct.2006.07.010>.
- [34] Wallach JC, Gibson LJ. Mechanical behavior of a three-dimensional truss material. *Int J Solids Struct* 2001;38(40–41):7181–96.
- [35] Karakoç A, Santaoja K, Freund J. Simulation experiments on the effective in-plane compliance of the honeycomb materials. *Compos Struct* 2013;96:312–20. <http://dx.doi.org/10.1016/j.compstruct.2012.09.021>.
- [36] Tauhiduzzaman M, Carlsson LA. Influence of constraints on the effective in-plane extensional properties of honeycomb core. *Compos Struct* 2019;209(April 2018):616–24. <http://dx.doi.org/10.1016/j.compstruct.2018.10.080>.
- [37] van Bree SE, Rokoš O, Peerlings RH, Doškář M, Geers MG. A Newton solver for micromorphic computational homogenization enabling multiscale buckling analysis of pattern-transforming metamaterials. *Comput Methods Appl Mech Engrg* 2020;372. <http://dx.doi.org/10.1016/j.cma.2020.113333>, arXiv:2008.12850.
- [38] Xu R, Yang J, Yan W, Huang Q, Giunta G, Belouettar S, Zahrouni H, Zineb TB, Hu H. Data-driven multiscale finite element method: From concurrence to separation. *Comput Methods Appl Mech Engrg* 2020;363:112893. <http://dx.doi.org/10.1016/j.cma.2020.112893>.
- [39] Huang W, Xu R, Yang J, Huang Q, Hu H. Data-driven multiscale simulation of FRP based on material twins. *Compos Struct* 2021;256(September 2020):113013. <http://dx.doi.org/10.1016/j.compstruct.2020.113013>.
- [40] Bodaghi M, Damanpack AR, Hu GF, Liao WH. Large deformations of soft metamaterials fabricated by 3D printing. *Mater Des* 2017;131(April):81–91. <http://dx.doi.org/10.1016/j.matdes.2017.06.002>.
- [41] Gibson L, Ashby M. *Cellular solids structures and properties*. Cambridge University Press; 1999.
- [42] Hassani B, Hinton E. A review of homogenization and topology optimization II - Analytical and numerical solution of homogenization equations. *Comput Struct* 1998;69(6):719–38. [http://dx.doi.org/10.1016/S0045-7949\(98\)00132-1](http://dx.doi.org/10.1016/S0045-7949(98)00132-1).
- [43] Ongaro F. Estimation of the effective properties of two-dimensional cellular materials: a review. *Theor Appl Mech Lett* 2018;8(4):209–30. <http://dx.doi.org/10.1016/j.taml.2018.04.010>.
- [44] Zhang K, Deng Z, Meng J, Xu X, Wang Y. Symplectic analysis of dynamic properties of hexagonal honeycomb sandwich tubes with plateau borders. *J Sound Vib* 2015;351:177–88. <http://dx.doi.org/10.1016/j.jsv.2015.04.012>.
- [45] Sun WQ, Cheng W. Finite element model updating of honeycomb sandwich plates using a response surface model and global optimization technique. *Struct Multidiscip Optim* 2017;55(1):121–39. <http://dx.doi.org/10.1007/s00158-016-1479-1>.
- [46] Mukhopadhyay T, Adhikari S, Alu A. Probing the frequency-dependent elastic moduli of lattice materials. *Acta Mater* 2019;165:654–65.
- [47] Sa A, Tm B, Xi C. Broadband dynamic elastic moduli of honeycomb lattice materials: A generalized analytical approach. *Mech Mater* 2021.
- [48] Hashin Z, Shtrikman S. A variational approach to the theory of the elastic behaviour of multiphase materials. *J Mech Phys Solids* 1963;11(2):127–40. [http://dx.doi.org/10.1016/0022-5096\(63\)90060-7](http://dx.doi.org/10.1016/0022-5096(63)90060-7).
- [49] Malek S, Gibson L. Effective elastic properties of periodic hexagonal honeycombs. *Mech Mater* 2015;91:226–40.
- [50] Yang P, Hu N, Guo X, Dong L, Chen Y, Guo Z. An ultra-simple universal model for the effective elastic properties of isotropic 3D closed-cell porous materials. *Compos Struct* 2020;249(June):112531. <http://dx.doi.org/10.1016/j.compstruct.2020.112531>.
- [51] Kolouek V. Anwendung des gesetzes der virtuellen verschiebungen und des reziprozitätssatzes in der stabwerksdynamik. *Ing-Arch* 1941;12(6):363–70.
- [52] Banerjee JR, Sobey AJ. Dynamic stiffness formulation and free vibration analysis of a three-layered sandwich beam. *Int J Solids Struct* 2006;42(8):2181–97.
- [53] Banerjee JR, Gunawardana WD. Dynamic stiffness matrix development and free vibration analysis of a moving beam. *J Sound Vib* 2007;303(1–2):135–43.
- [54] Kennedy D. Dynamic stiffness analysis of graphene sheets and carbon nanotubes. *Civ-Comp Proc* 2012;99:1–12. <http://dx.doi.org/10.4203/ccp.99.99>.
- [55] Liu X, Liu X, Adhikari S, Zhao X. An analytical framework for broadband dynamic analysis of plate built-up structures with uncertain viscoelastic boundary or connection conditions. *Mech Syst Signal Process* 2022;177(November 2021):109121. <http://dx.doi.org/10.1016/j.ymssp.2022.109121>.
- [56] Liu X, Chang L, Banerjee JR, Dan HC. Closed-form dynamic stiffness formulation for exact modal analysis of tapered and functionally graded beams and their assemblies. *Int J Mech Sci* 2022;214(July 2021):106887. <http://dx.doi.org/10.1016/j.ijsolstr.2021.106887>.
- [57] Liu X, Zhao Y, Zhou W, Banerjee JR. Dynamic stiffness method for exact longitudinal free vibration of rods and trusses using simple and advanced theories. *Appl Math Model* 2022;104:401–20. <http://dx.doi.org/10.1016/j.apm.2021.11.023>.
- [58] Liu X, Liu X, Adhikari S, Yin S. Extended Wittrick-Williams algorithm for eigenvalue solution of stochastic dynamic stiffness method. *Mech Syst Signal Process* 2022;166(March 2021):108354. <http://dx.doi.org/10.1016/j.ymssp.2021.108354>.
- [59] Liu X, Qiu S, Xie S, Banerjee JR. Extension of the wittrick-williams algorithm for free vibration analysis of hybrid dynamic stiffness models connecting line and point nodes. *Mathematics* 2022;10(1). <http://dx.doi.org/10.3390/math10010057>.
- [60] Liu X, Zhao X, Liu X. A highly accurate spectral dynamic stiffness method for efficient broadband modal and dynamic response analysis of membranes assemblies with arbitrary boundary conditions. *Comput Struct* 2022;267:106797.
- [61] Catapano A, Montemurro M. A multi-scale approach for the optimum design of sandwich plates with honeycomb core. Part I: Homogenisation of core properties. *Compos Struct* 2014;118(1):664–76. <http://dx.doi.org/10.1016/j.compstruct.2014.07.057>.
- [62] Huang T, Gong Y, Zhao S. Effective in-plane elastic modulus of a periodic regular hexagonal honeycomb core with thick walls. *J Eng Mech* 2018;144(2):06017019. [http://dx.doi.org/10.1061/\(asce\)em.1943-7889.0001412](http://dx.doi.org/10.1061/(asce)em.1943-7889.0001412).

- [63] Mukhopadhyay T. Theoretical limits for negative elastic moduli in subacoustic lattice materials. *Phys Rev B* 2019;094108:1–7.
- [64] Li Y, Abbès F, Hoang MP, Abbès B, Guo Y. Analytical homogenization for in-plane shear, torsion and transverse shear of honeycomb core with skin and thickness effects. *Compos Struct* 2016;140:453–62.
- [65] Tao Y, Duan S, Wen W, Pei Y, Fang D. Enhanced out-of-plane crushing strength and energy absorption of in-plane graded honeycombs. *Composites B* 2017;118:33–40.
- [66] Guo Z, Wang L, Chen Y, Zheng L, Yang Z, Dong L. A universal model for predicting the effective shear modulus of two-dimensional porous materials. *Mech Mater* 2017;110:59–67. <http://dx.doi.org/10.1016/j.mechmat.2017.04.006>.
- [67] Deshpande VS, Fleck NA, Ashby MF. Effective properties of the octet-truss lattice material. *J Mech Phys Solids* 2001;49:1747–69.
- [68] Scarpa F. Elastic buckling of hexagonal chiral cell honeycombs. *Composites A* 2007;38:280–9.
- [69] Liu X, Sun C, Banerjee JR, Dan H-C, Chang L. An exact dynamic stiffness method for multibody systems consisting of beams and rigid-bodies. *Mech Syst Signal Process* 2021;150:107264.
- [70] Rathbun HJ, Radford DD, Xue Z, He MY, Yang J, Deshpande V, Fleck NA, Hutchinson JW, Zok FW, Evans AG. Performance of metallic honeycomb-core sandwich beams under shock loading. *Int J Solids Struct* 2006;43:1746–63.
- [71] Deshpande VS, Fleck NA, Evans AG. The out-of-plane compressive behavior of metallic honeycombs. *Mater Sci Eng A* 2004;380:272–80.
- [72] Wan H, Ohtaki H, Kotosaka S, Hu G. A study of negative Poisson's ratios in auxetic honeycombs based on a large deflection model. *Eur J Mech A Solids* 2004;23:95–106.
- [73] Yang L, Harrysson O, West H, Cormier D. Mechanical properties of 3D re-entrant honeycomb auxetic structures realized via additive manufacturing. *Int J Solids Struct* 2015;69–70:475–90.
- [74] Mousanezhad D, Babae S, Ebrahimi H, Ghosh R. Hierarchical honeycomb auxetic metamaterials. *Nature Publishing Group*; 2015, p. 1–8.
- [75] N. Gaspar, X.J. Ren b, C.W. Smith, J.N. Grima KE. Novel honeycombs with auxetic behaviour. *Acta Mater* 2005;53:2439–45.
- [76] Abramovitch H, Burgard M, Edery-Azulay L, Evans KE, Hoffmeister M, Miller W, Scarpa F, Smith CW, Tee KF. Smart tetrachiral and hexachiral honeycomb: Sensing and impact detection. *Compos Sci Technol* 2010;70(7):1072–9. <http://dx.doi.org/10.1016/j.compscitech.2009.07.017>.
- [77] Leung AYT. *Dynamic stiffness and substructures*. Springer London; 1993.
- [78] Paz M. *Structural dynamics: Theory and computation*. Van Nostrand, Reinhold.